Chronic Ethanol Exposure Produces Persistent Impairment in Cognitive Flexibility and Decision Signals in the Striatum

Yifeng Cheng[1], Robin Magnard[1], Angela Langdon[2], Daeyeol Lee[1,3,4,5], and Patricia H. Janak[1,4,5]

[1]Department Psychological and Brain Sciences, Krieger School of Arts and Sciences, Johns Hopkins University, Baltimore, MD;
[2]Intramural Research Program, National Institute of Mental Health, National Institutes of Health, Bethesda, MD;
[3]Zanvyl Krieger Mind/Brain Institute, Krieger School of Arts and Sciences, Johns Hopkins University, Baltimore, MD;
[4]Department of Neuroscience, Johns Hopkins University School of Medicine, Baltimore, MD;
[5]Kavli Neuroscience Discovery Institute, Johns Hopkins University, Baltimore, MD.

***Correspondence:**
Patricia Janak, Ph.D.
3400 N Charles Street,
Dunning Hall 246,
Baltimore, MD 21218
E-mail: patricia.janak@jhu.edu

ABSTRACT

Lack of cognitive flexibility is a hallmark of substance use disorders and has been associated with drug-induced synaptic plasticity in the dorsomedial striatum (DMS). Yet the possible impact of altered plasticity on real-time striatal neural dynamics during decision-making is unclear. Here, we identified persistent impairments induced by chronic ethanol (EtOH) exposure on cognitive flexibility and striatal decision signals. We showed that after a substantial withdrawal period of EtOH vapor exposure, rats exhibited reduced adaptability and exploratory behavior during a dynamic decision-making task. Reinforcement learning models showed that repeated EtOH exposure enhanced learning from rewards over omissions, leading to increased relative value updates on the selected action. Notably, neural signals in the DMS related to the decision outcome were enhanced, while those related to choice and choice-outcome conjunction were reduced, in EtOH-treated rats compared to the controls. These findings highlight the profound impact of chronic EtOH exposure on adaptive decision-making, pinpointing specific changes in striatal representations of actions and outcomes as underlying mechanisms for cognitive deficits.

INTRODUCTION

Cognitive flexibility enhances survival by facilitating adaptation to changing environments and improving outcomes in an ever-changing world. The ability to make flexible decisions is substantially altered by chronic ethanol (EtOH) use and dependence across species, impairing goal-directed behavior while enhancing habitual or stimulus-orientated behavior[1-7]. Low cognitive flexibility may contribute to future escalation of substance use[8-10], including EtOH intake in both rodents and primates[11-14] and in heightening the risk of relapse to alcohol use in humans[15, 16].

Cognitive flexibility, evaluated through reversal learning tasks[17, 18], involves learning beneficial choice and adapting to new action-outcome contingencies. Although the cognitive and neural mechanisms underlying chronic EtOH-induced reversal deficits are not yet fully understood, studies in humans have shown persistent disruption of reversal learning during protracted withdrawal from EtOH drinking[19-22]. In rodents, while EtOH exposure in adolescent subjects results in persistent cognitive deficits[23, 24], studies to date of chronic EtOH exposure and cognitive flexibility in adult rodents report relatively short-lasting (~$\leq$ 2 weeks) deficits[25-28], or no deficits[24, 29-31]. Thus, it remains unclear whether chronic EtOH exposure in adults causes a persistent deficit in flexible decision-making, despite evidence of such deficits in humans.

Corticostriatal circuitry is implicated in decision flexibility[32, 33]. In our previous studies, we found that chronic EtOH use evoked maladaptive striatal synaptic plasticity[34-39], particularly in the dorsomedial striatum (DMS), that persist several weeks[40], in agreement with other recent work[3]. Thus, we hypothesize that repeated exposure to EtOH vapor induces abnormal corticostriatal synaptic plasticity that disrupts striatal neural activity,

63 leading to a persistent loss of cognitive flexibility.

64 In the current study, we confirmed that chronic EtOH-elicited deficits after protracted
65 withdrawal in adults do not manifest in standard two-bandit probabilistic reversal learning
66 (PRL)[41, 42]. Thus, we devised a PRL task that requires rats to establish and update
67 knowledge of reward probabilities under different levels of uncertainties. With this new
68 task, we found EtOH-induced behavioral change across multiple behavioral measures,
69 including overall measures of the exploration-exploitation trade-off and reversal deficits
70 in highly uncertain environments. In addition, these deficits were found only in male, not
71 female, rats. Using a reinforcement learning framework, we found that EtOH-dependent
72 subjects showed specific alterations in differential value updating after receiving reward
73 or no reward, providing a potential computational explanation for the observed deficits.
74 Using *in vivo* electrophysiological recording within the DMS, we observed reduced
75 encoding of choice signals alongside an enhanced encoding of outcome signals.
76 Together, these findings reveal behavioral and neural mechanisms underlying the effects
77 of chronic EtOH during protracted withdrawal and suggest that altered striatal processing
78 of choice and outcome may contribute to EtOH-induced deficits in cognitive flexibility.

79 **RESULTS**

80 **Protracted withdrawal from chronic EtOH exposure produces a distinct**
81 **behavioral pattern in the dynamic PRL task**

82 To investigate whether chronic EtOH exposure disrupts decision-making beyond
83 the phase of acute withdrawal (>1 week), we used a well-validated chronic intermittent
84 EtOH (CIE) vapor procedure to model EtOH dependence in rats[3, 43, 44]. Rats were trained
85 on a standard probabilistic reversal learning (PRL) task and then underwent cycles of

86 EtOH or air vapor exposure and withdrawal for four weeks (16 hrs/day, 5 days/wk), with
87 group assignment balanced for PRL performance. Following 10-15days of withdrawal,
88 performance on the standard PRL task was reassessed (Figure S1A). This task required
89 water-restricted rats to earn a drop (33 μl) of 10% sucrose water by choosing between
90 left and right levers, which delivered a reward with either a 70% or a 10% probability,
91 while the reward probabilities repeatedly switched within a session (Figure S1B). Previous
92 studies have failed to find effects of the CIE procedure in adult rats on learning
93 performance in the operant reversal task[29, 30]. Indeed, during this standard PRL task, we
94 did not observe any significant differences in reversal learning after block switches when
95 comparing within-subject performance before and after CIE procedure (Figure S1C-1G),
96 nor between EtOH and air controls in either male or female (Figures S1C-1G) rats. To
97 further understand whether the CIE procedure could induce overall behavioral changes
98 across multiple behavioral measures, we employed a Support Vector Machine analysis
99 (SVM)[45-47] to decode group membership from a high-dimensional behavioral dataset
100 consisting of 20 behavioral measures gathered during pre- and post-reversal phases in
101 EtOH rats and their air controls (Figure S2A). We found that trained SVM models could
102 not identify either group labels or sex labels in pre- and post-vapor behavior in this PRL
103 task above chance level (Figure S2B). These findings indicate that rats did not express
104 obvious EtOH-induced performance changes within the standard PRL task.

105 To further explore possible effects of chronic EtOH on cognitive flexibility, we next
106 modified the task to present greater cognitive challenge[48, 49]. We introduced a three-block
107 design with reward probabilities that varied in the contrast between left and right lever
108 probabilities (80:10, 60:30, and 45:45; Figure 1C), converting the standard PRL task into

109 a dynamic PRL task (dynaPRL). Consequently, when blocks transitioned from one to
110 another, rats faced different amounts of uncertainty such that a larger change in the
111 reward probabilities would be easier to detect and might facilitate the adaptive changes
112 in the animal's behavior (Figure 1C). Visual inspection of the trial-by-trial performance of
113 individual rats in both air and EtOH groups revealed that subjects adjusted their choice
114 behavior in response to block transitions within the dynaPRL task (Figure 1D). Applying
115 the same SVM model to the same behavioral features used for the analysis of behavioral
116 data from the standard PRL task (Figure 1E), we found that for the dynaPRL task, the
117 model could decode group (air v.s. EtOH) and sex labels from the behavioral dataset with
118 a prediction precision (63.29%) significantly higher than chance levels (25%; $p < 0.001$).
119 The trained SVM decoder almost never (<0.001% chance) misclassified male and female
120 subjects (Figure 1G). More importantly, the decoding accuracy for the EtOH treatment
121 was significantly higher than chance level for male but not female rats (Figure 1F). Using
122 uniform Manifold Approximation Projection (UMAP), we found that the data were distinctly
123 segregated between male EtOH and air rats in a 2D low-dimensional space with an
124 accuracy (~70%), similar to the SVM decoding in predicting group membership (Figure
125 1G).

126 Taken together, these results indicate that the impact of prior chronic EtOH
127 exposure can be detected in male rats many weeks (>10 wks) after the last EtOH
128 exposure through multivariate analysis of high dimensional behavioral measures during
129 the more challenging dynaPRL decision-making task.
130

131 **Chronic EtOH exposure slows reversal learning and reduces exploration**

132 The SVM analysis showed that behavior of male EtOH-exposed rats in the
133 dynaPRL task differed from control rats. To understand the basis for this difference, we
134 first examined how male EtOH and air rats adjust their choice behavior in response to
135 changes in reward probabilities upon block switch. We analyzed the probability of
136 selecting the action that was advantageous before the reversal. When a block switched
137 from low uncertainty to high uncertainty (Lo-Hi) (Figure 2A), a two-way mixed-effect
138 ANOVA revealed a significant interaction between group and trials in males (Figure 2B;
139 $p = 0.016$). Bonferroni post-hoc tests showed that male EtOH rats were significantly more
140 likely to choose the previously preferred action in trials 2~5 after the block transition than
141 the rats in the air control group. To quantify this further, we fit a single-exponential decay
142 model to the probability of choosing the previously preferred action across the first 12
143 trials post-block transition (Figure 2C). While there was no difference in pre-reversal
144 asymptotic value (*a)* or the magnitude of change in learning new action-outcome
145 contingency after the reversal (*d*) (Figures 2D and 2E), we observed a lower adaptation
146 rate (λ) in EtOH rats compared to the controls (Figure 2F; $p = 0.016$). Given that the
147 inverse of λ ($\tau = 1/\lambda$) corresponds to the time constant of the rat's learning in a new block,
148 this indicates that EtOH rats needed more experience to adapt to a new contingency in a
149 highly ambiguous environment (Figure 2G; $p = 0.036$). Additional analyses applied to
150 single sessions and individual rats revealed the same pattern of results (Figure S3A). By
151 contrast, these effects were not observed during block transitions from high to low
152 uncertainty (Hi-Lo), at the same uncertainty level before and after block transitions
153 (same), or when all trial types were combined (Figures S3B-3D and S4A-S4F). Such

154 findings suggest that the impact of EtOH on reversal learning dynamics is prominent only
155 when facing a sudden transition to high uncertainty. To examine choice behavior later in
156 a block, after rats are expected to have acquired the new contingencies, we focused on
157 behavior >12 trials from block switch and assessed how much choice probability deviated
158 from local reward rate yielded by the choice ('matching behavior')[50]. Male EtOH rats
159 aligned their choices with local reward rates more tightly than same-sex control rats
160 (Figure S5A-S5D).

161 To investigate strategies that might underlie the EtOH-induced choice behavior
162 deficits, we analyzed behavioral metrics in two key phases, the early reversal learning
163 phase, including trials 2 to 7 (*t*2-*t*7) after transitioning to a new block, and the late phase
164 of the current block, spanning the last 6 trials (*t*-6 to *t*0) before block switch. We found
165 that male EtOH rats were more likely to repeat the same choice in consecutive trials in
166 the early phase following a switch, but not in the late phase after rats have adapted to the
167 contingency change, as shown by measures of stay probabilities and the differences
168 between win-stay and lose-shift probabilities (Figures 2H-2J and S6A-S6H). This
169 behavior was sensitive to the receipt or omission of reward; EtOH rats exhibited higher
170 stay probabilities after reward omission, but not reward receipt, during 'Lo-Hi' transitions
171 (Figure 2I), resulting in a more tendency of win-stay and less lose-shift (Figure 2J). We
172 additionally found evidence that chronic EtOH exposure impacted deliberation processes,
173 as revealed by alternations in latencies for trial initiation and choice during early reversal.
174 Male EtOH rats were faster to initiate a new trial following a reward omission in the
175 previous trial (Figure S7A-S7H) and had overall shorter latencies when making their
176 choice, which was less modulated by the current action strategy (stay or switch) they held

177 (Figures S8A-S8H). In contrast to males, female EtOH exposed rats did not show
178 alternations in reversal behavior, matching behavior, win-stay behavior, or response
179 latencies (Figures S4G-S4H, S5E-S5H, S6I-S6P, S7I-S7P, and S8I-S8P).

180 Collectively, these results demonstrate that chronic EtOH exposure significantly
181 impacted outcome-driven action strategies, favoring a shift from switch to stay and
182 enhancing matching behaviors in male rats, i.e., a tendency for greater exploitation and
183 less exploration, resulting in a reduction in cognitive flexibility during a dynamic decision-
184 making task.

185 **Chronic EtOH exposure alters value updating in reinforcement learning**

186 To better understand the computational processes underlying the observed EtOH-
187 induced alternations in decision-making, we applied several reinforcement learning (RL)
188 models to the trial-by-trial choice and reward data. We found that a Q-learning model with
189 differential learning rates (model 2, Q-DFLr) outperformed all other candidate models
190 (Figure S9A). Q-DFLr has four distinct learning parameters controlling the updating of the
191 value function: α^+ and α^- for updating the value of chosen actions when the outcome of
192 the action is reward or no reward, respectively, and θ^+ and θ^- for discounting the value of
193 unchosen actions when the outcome of the action is reward or no reward, respectively
194 (Figure 3A). To assess the group-level differences between the EtOH group and the air
195 control across RL parameters, we constructed a hierarchical model wherein the
196 distributions of individual parameters for each rat are determined by the group-level
197 hyperparameters. These hyperparameters encompass the means of the distributions for
198 each parameter, the mean differences (δ) between air and EtOH groups for each
199 parameter, and the variances of each parameter's distribution. The posterior density of

these hyperparameters was estimated through sampling using Hamiltonian Markov Chain Monte Carlo (HMC) methods. We found that distributions of group differences, δ, for α^+ and θ^- substantially shifted towards the positive direction, indicating EtOH group has a higher α^+ and θ^- value than those in air group (Figures 3B and 3C). We quantified the magnitude of evidence for group differences using directed Bayes Factor (dBF) and discovered that the likelihood of an increase in α^+, the learning rate when rewarded, in the EtOH group was approximately 6-fold higher than a decrease (Figure 3B; dBF = 6.01). Similarly, for the EtOH group, the forgetting rate in the absence of reward, θ^-, was roughly 8-fold more likely to increase than decrease (Figure 3C; dBF = 8.35). All other parameters showed lower differences between the two groups (Figure S9B; all dBFs < 1).

We then used the best-fit parameters to simulate choice behavior within the original block structure used in the experiment and analyzed the probabilities of perseveration for each block transition type. We found that the simulated data partially recapitulated the EtOH-induced reversal deficits observed when transitioning from a low to a high uncertainty block in the empirical data, but not for other types of block transitions (Figures 3D and S9C). Collectively, these data suggest that chronic EtOH exposure selectively enhanced both reward-based updates for selected actions and the omission-based forgetting of unselected options, biasing action-selection towards previously reinforced choices. These results provide an algorithmic explanation for the changes in choice behavior we observed.

220 **Prior EtOH exposure alters the recruitment of DMS neurons representing choice**
221 **and reward**

222 Our behavioral analyses indicated that EtOH and air-control rats showed
223 differences in action value updating, and this might reflect alterations in neural activity
224 related to outcome processing. We therefore sought to examine the impact of EtOH on
225 DMS neural dynamics during outcome presentation, defined as the 1000ms after the
226 outcome (reward or reward omission) was revealed, in dynaPRL. We recorded a total of
227 524 and 326 single units in the DMS from EtOH and air groups, respectively (Figure S10).
228 Using regression models, we first examined how neural activity in different time epochs
229 throughout the trial was affected by the animal's choice, the outcome of the choice, and
230 their interaction, in the current trial (t) and previous trial (t-1). While choice-related signals
231 were apparent in both groups throughout the trial (Figure S11A), a lower fraction of
232 choice-modulated neurons was observed in EtOH rats than in control rats during the
233 outcome presentation (Figures 4A, 4E, and S11A; $p = 0.021$ for 4E). Conversely, a larger
234 portion of DMS neurons (~80%) was significantly modulated by the outcome in EtOH rats
235 than in rats from air control group (Figures 4B, 4F, S11C; $p = 0.018$ for 4F). Further
236 analysis into whether EtOH exposure affects the striatal representation of choice-outcome
237 conjunction or the value of chosen actions during the outcome presentation phase
238 revealed no significant group differences in these neural representations (Figures 4C, 4D,
239 4G, 4H, and S11E).

240 The regression coefficients obtained from this analysis measure the impact of each
241 decision variable on the neural firing rate during the period of outcome presentation.
242 Given that the magnitude of these regression coefficients varied over time, Principal

243 Component Analysis (PCA) was applied to the signed regression coefficients across time
244 bins for each neuron. The magnitudes of the first principal component (PC1) scores were
245 then utilized as an index of modulation strength over time. We found that choice and
246 choice-outcome interaction signals have a significantly greater modulation strength on
247 striatal firing activity from air rats compared to EtOH rats (Figures 4I and 4K; $p = 0.049$
248 and 0.0004, respectively), whereas outcome signals have a significantly greater
249 modulatory effect on neural activity from EtOH rats compared to air controls (Figure 4J;
250 $p = 0.041$). No difference was observed for the chosen value in modulating striatal firing
251 (Figure 4L). While we found a significant impact of the previous trial's outcome on neural
252 activity within the trial, there was no evidence for group differences (Figures S11B, S11D,
253 and S11F).

254 Collectively, these results demonstrate that a higher proportion of DMS neurons
255 from EtOH rats encoded immediate outcome, whereas the signals related to current
256 choice and action-outcome contingency were reduced relative to air controls.

257 **Action-selection value signals distinctly modulate DMS neuronal activity**

258 Next, we evaluated whether EtOH impacted how value signals were encoded in
259 the DMS during the action selection phase, defined as the time period from trial initiation
260 until lever press. In particular, we sought to quantify the strength and time course of
261 striatal activity related to two orthogonal combinations of the action values[52] estimated by
262 the best-fitting reinforcement learning model (model 2, Q-DFLr). The first variable
263 corresponds to the difference between the two available action values, ΔQ, which is
264 monotonically related to the probability of pressing the lever ipsilateral to the electrodes
265 and is referred to as the policy. The second variable is the summation of the two available

266 action values; ΣQ, and roughly corresponds to the so-called state value. We analyzed
267 neural firing rates, aligned with either trial initiation, lever insertion, or lever press, as linear
268 functions of ΔQ and ΣQ, with choice and chosen action value included as control variables
269 in the regression analysis. We found that even several hundred milliseconds prior to trial
270 initiation, a small (~15%) but significant proportion of striatal neurons from air control rats
271 changed their spike rate in response to ΣQ (state value), and this state signal persisted
272 until at least 200ms after trial initiation (Figures 5A and 5G). In contrast, the state value-
273 sensitive neural population was much smaller in the EtOH rats (Figure 5G; $p = 0.004$).
274 Thereafter, the proportion of neurons from both groups modulated by state value became
275 similar in the two groups, and the state value signals decreased close to chance levels
276 during the lever insertion time epoch (Figures 5B and 5H) and increased again after lever
277 press (Figures 5C and 5I).

278 Additionally, a small proportion of neurons (~10%) encoded ΔQ (policy) starting
279 before trial initiation and the fraction of these policy-coding neurons increased to about
280 15% until the completion of the lever press in air controls (Figures 5D, 5E, 5F, 5J, 5K,
281 and 5L). There were no significant between-group differences in the proportion of neurons
282 encoding policy during the trial epochs, although there was a tendency for a smaller
283 proportion of policy-encoding striatal neurons in the EtOH rats than in the air controls
284 when the spike rate was aligned to the lever press (Figure 5L; $p = 0.053$). These results
285 suggest that EtOH differentially alters the neural representation of states selectively in the
286 distal action selection phase (i.e., trial initiation) and possibly of action policies in the
287 proximal action selection phase (i.e., lever press).

288

DISCUSSION

In this study, we show that chronic EtOH vapor exposure during adulthood induces long-lasting (>10 weeks withdrawal) behavioral deficits in rats in a sex-specific manner. Behavioral data obtained during performance of a dynamic probabilistic reversal learning task (dynaPRL) could be used to predict group membership of EtOH-exposed vs air-exposed male subjects. Examination of the data revealed that cycles of high-dose EtOH exposure impaired later reversal learning under high uncertainty and led to an overall propensity to repeat a given choice, regardless of outcome, in male, but not female, rats. We employed a reinforcement learning model to elucidate underlying mechanisms for our observed behavioral deficits and found that the reward-mediated learning rate, which updates the value of chosen actions, and the reward omission-mediated forgetting rate that regulates the decay over time of the unchosen action value, were both increased in male rats exposed to chronic intermittent EtOH vapor. Lastly, EtOH exposure reconfigured firing patterns of dorsomedial striatum (DMS) neurons in male rats, augmenting neuronal sensitivity to the outcome while diminishing responsiveness to the choice, policy, and state signals. Our findings shed light on the cognitive and neural computational mechanisms underlying drug-induced persistent deficits in cognitive flexibility.

Research on the effect of chronic EtOH consumption has presented a nuanced landscape across species. In humans, chronic EtOH abuse and withdrawal have been linked to marked neuropsychological impairments[22, 53-56], with several studies highlighting cognitive deficits following moderate to extended periods of withdrawal[20, 21, 57-62]. Contrastingly, in rodents, while some long-lasting effects on goal-directed control[3, 63] and

312 working memory[64] are noted, the evidence for impacts on reversal learning and
313 attentional tasks has been inconsistent[24-31, 65]. This discrepancy between human and
314 animal studies may stem from differences in longer EtOH use or poly-substance use[66]
315 histories in humans and more complex cognitive demands of human tasks compared to
316 rodent models. For example, the Wisconsin card sorting task involves complex rule shifts,
317 unlike simpler rodent reversal learning tasks[33, 40-42, 67, 68]. Our findings from a standard
318 probabilistic reversal learning (PRL) task showed no significant behavioral differences pre
319 and post EtOH exposure, aligning with prior studies in both rodents[29, 30] and humans[69].
320 However, by varying uncertainty in reward probabilities in an adjusted dynaPRL task[48, 49]
321 and hence enhancing its complexity and challenge, we uncovered more reliable EtOH-
322 induced cognitive deficits.

323 When facing sudden cognitive challenges in the dynaPRL task, EtOH rats
324 exhibited a robust deficit in reversal learning, i.e., a higher probability of repeating their
325 choice, especially after reward omission in a high-uncertainty environment. Additionally,
326 EtOH rats exhibited less deviation from matching their choices to the inferred reward
327 schedule[51]. These findings suggest that EtOH rats might favor exploitation over
328 exploration, in line with human studies[70]. Exploration-exploitation behaviors are
329 modulated by novelty and uncertainty[71]. A plausible explanation for the reduction in
330 exploration might be that EtOH pre-exposure diminishes outcome sensitivity. If true, a
331 change in exploration across all other uncertainty conditions would be expected. However,
332 this effect was observed only after transitioning from a low to high uncertainty
333 environment. Therefore, another interpretation consistent with the current findings is that
334 chronic EtOH exposure either decreases uncertainty-mediated exploration[72] or promotes

335 uncertainty avoidance following unrewarded choices, independent of learning[71]. Humans
336 with EtOH use disorder display aberrant decision-making amidst high ambiguity in the
337 Iowa Gambling Task[73, 74] The intolerance of uncertainty has also been associated with
338 risky EtOH use behavior[75] and "hyperkatifeia"[76]. EtOH-exposed rats also exhibited shorter
339 response times in the dynaPRL task across all block transitions (a change therefore
340 independent of uncertainty) during protracted withdrawal. This observation aligns with
341 increased impulsivity observed in humans with alcohol use disorder[77-79]. Thus, we
342 identified multiple behavioral changes during protracted EtOH withdrawal in male rats.

343 We also found that male rats are more vulnerable to the negative impacts of
344 chronic EtOH vapor exposure than female rats during the dynaPRL task. This is in line
345 with previous literature that CIE vapor in adults rats impairs goal-directed behavior in
346 males but not females[80]. Although Aguiree et al.[30] showed females are more vulnerable
347 to chronic EtOH use in early reversal learning, this may be due to the fact that females
348 consumed more EtOH than males in their study, whereas the vapor exposure method
349 produced similar blood EtOH levels in both males and females in our study, as in that of
350 Barker and colleagues[80]. Estrogen potentially induces neuroprotective and anti-
351 inflammatory effects[81, 82] in chronic EtOH vapor-exposed female rats and facilitates
352 recovery during the protracted withdrawal phase. However, this cannot fully explain the
353 differences in behavior between males and females in air controls. We speculate that the
354 observed sex-related differences in response to uncertainty, particularly under stress,
355 may stem from inherent variations in how males and females process uncertainty[83].
356 However, more studies are needed to understand how EtOH-induced cognitive
357 impairments in a sex-dependent manner.

358 Reinforcement learning theory provides a theoretical framework for describing the
359 cognitive process of value-based decision-making[84] and has been informative for the
360 dissection of pathological decision processes in animal models of addiction[85]. Our
361 observations in EtOH-dependent rats align well with findings from a human study utilizing
362 a Q-learning model, which identified EtOH-dependent individuals are associated with
363 decreased in sensitivity of reward omission and increased sensitivity to reward[86].
364 Similarly, in our study, a history of chronic exposure enhanced the updating of chosen
365 value upon receiving rewards, indicating heightened reward sensitivity. It also facilitated
366 the decay of unchosen value when unrewarded, reflecting a diminished emphasis on
367 negative feedback. As a result, EtOH exposure heightened the emphasis on selected
368 actions regardless of their outcomes, leading to increased behavioral exploitation. This
369 provides a computational mechanism that explains our observations of EtOH-induced
370 behavioral perseveration.

371 Numerous studies have shown one of DMS's critical roles in encoding decision-
372 related variables[32, 52, 87-94] and controlling action selection in value-based decision tasks[41,
373 95-100]. Expanding upon the findings from earlier research [91, 93], our results demonstrate
374 that dorsomedial striatal (DMS) neurons in rats from EtOH and air groups encode a
375 preparatory choice signal at least few hundreds milliseconds before trial initiation, peaking
376 at the onset of outcome, and then diverging in EtOH and air treated rats, with reduced
377 choice encoding in EtOH rats. During the same outcome presentation period, encoding
378 of the outcome is enhanced in EtOH rats. The observed aberrant attenuation in choice
379 signals and augmentation of outcome signals during the outcome presentation period
380 induced by EtOH exposure may disrupt contingency learning processes. As anticipated,

choice-outcome conjunction signals emerge post-reward onset and are impaired in rats with chronic EtOH pre-exposure. State values approximate how often an animal has been rewarded recently[52], which is likely to be important environmental information for inferring the block type. Although each block has the same averaged reward probabilities, the local reward rate reflects the uncertainty level of the block (Figure S12). Our findings show suppressed state value representations at trial start in EtOH rats, which may disrupt the animal's inference regarding the block transitions.

Our findings offer novel *in vivo* evidence that chronic EtOH exposure engenders enduring alterations in neurocomputational processes. It is possible the aberrant neural activity changes in the DMS might stem from a combination of EtOH-induced maladaptive plasticity both in the corticostriatal pathway and in the nigrostriatal DA pathway. Prior studies found that chronic EtOH consumption and withdrawal induce aberrant orbito-striatal plasticity in the DMS[3, 37, 101, 102]. These orbitofrontal cortical inputs are proposed to encode various aspects of expected value[103-106] and goal-directed choice and action-outcome associations[107-110], respectively. Additionally, EtOH has been reported to disturb dopamine homeostasis in the striatum[111, 112].

In summary, this study has unveiled specific and enduring behavioral and neural consequences of chronic EtOH exposure, providing new insights into mechanisms underlying cognitive impairments associated with EtOH addiction. Chronic EtOH consumption appears to distort neural computational processes, potentially interfering with the representation of decision-making signals, leading to cognitive inflexibility. These mechanisms may underline some of the deficits observed in humans with alcohol use disorder. Importantly, behavioral and neural mechanisms for the changes we observed

404 here after chronic EtOH might resemble those underlying loss of cognitive flexibility after

405 chronic use of other drugs of abuse[113] or other psychiatric disorders[114-116].

406

407 **MATERIALS AND METHODS**

408 **Animals**

409 17 Male and 10 female Long-Evans (LE) rats (10 wks old upon arrival, Envigo)
410 were singly housed. Rats were kept in a temperature- and humidity-controlled
411 environment with a light:dark cycle of 12:12 h (lights on at 7:00 a.m.). Experiments were
412 conducted during their light cycle. All animal care and experimental procedures were
413 approved by the Johns Hopkins University Institutional Animal Care and Use Committee.

414 **Chronic intermittent EtOH vapor exposure (CIE)**

415 Rats were exposed to four rounds of EtOH vapor (n = 8 male and 5 female) or air
416 (n = 9 male and 5 female)[3, 44, 117, 118]. Each round consisted of 14 hrs of vapor exposure
417 followed by a 10-hr withdrawal, repeated for 5 consecutive days. EtOH was volatilized by
418 venting air through a heating flask containing 95% EtOH at a rate of 30-40 l/min. EtOH
419 vapor was delivered to rats housed in Plexiglas chambers (La Jolla Alcohol Research,
420 inc.). Blood was collected from the tip of tails in the middle and end of each round from
421 all EtOH-exposed rats to assess blood EtOH concentrations (BECs) with an AM1 alcohol
422 analyzer from Analox Inc. To control the stress level of the blood collection, we pinched
423 the tip of tails instead of cutting the tissue and collecting blood on air controls. Our
424 procedure produced a mean BEC of 224.95 $\pm$ 14.51 (S.E.M) in male and 257.2 $\pm$ 23.79
425 (S.E.M) mg/dl in female rats without significant sex differences (Figure 1A, inset), which
426 is in line with previous findings[3, 43, 44].

427 **Probabilistic reversal learning (PRL) task**

428 Rats undergoing behavioral testing were water-restricted to 90% of their *ad-libitum*
429 weight. Behavioral experiments were performed in a soundproof customized modular

430 operant chamber. The levers (MED Associates, ENV-112CM) and a reward magazine
431 were confined to the same wall of the chamber. Rats were initially trained to enter a
432 magazine to collect a reward by delivering a 100 µl reward (10% w/v sucrose in tap water)
433 at random times with an average interval of 60 s (RT60). Subsequently, the rats were
434 trained to initiate a trial by entering the magazine, which triggered the insertion of two
435 levers into the chamber. Pressing a lever would lead to a reward delivery (at this stage,
436 both levers provided a reward with a 100% probability). Lastly, rats were trained on the
437 final task, with pressing one lever consistently delivering a reward (100% probability), and
438 the other lever was not rewarded (0% probability). These action-outcome contingencies
439 were reversed randomly 8 trials after the value of exponential moving averaged past 8
440 choices (1 for correct and 0 for incorrect choice) crossed the 0.75 threshold. The block
441 reversal probability was 10%. If the block was not switched within 20 trials of crossing the
442 threshold, the computer forced the reversal. Thus, each rat had adequate trials to acquire
443 current contingencies and could not predict the contingency reversal. One to three days
444 after the deterministic reward schedule (100% and 0%) training, the reward probabilities
445 for each lever were selected between 70% and 10%. Each trial in the final task began
446 with the illumination of the reward magazine. Upon poke into the magazine detected by
447 an infrared head entry detector (MED Associates, ENV-254-CB) (trial initiation), two
448 levers flanking the left and right sides of the port were inserted after a variable delay
449 (randomly selected between 100 ms to 1 s with 100 ms intervals). Animals were given
450 30-s to press a lever; failure to do so resulted in an invalid trial (<1% of trials for all rats)
451 and was excluded from analysis. A lever press probabilistically resulted in either the CS-
452 (0.5 s of white noise generated by MED Associated, ENV-225SM) with no reward delivery

453 or the CS+ (two clicker sounds generated by MED Associated, ENV-135M) with ~33-μl
454 reward delivery in the center magazine via a syringe pump (MED Associated, PHM-100).
455 Each trial ended either at the end of the CS- presentation or after completing the reward
456 collection (exit from the first magazine entry after reward delivery). Trials were separated
457 by a constant 2.5-s intertrial interval. Rats were trained from Monday to Friday, and each
458 behavioral session lasted approximately two hours.

459 **Dynamic probabilistic reversal learning (dynaPRL) task**

460 Water-restricted rats performed this task in the same operant chamber as in the
461 original PRL task. The task structure was the same as PRL task except that reward
462 probabilities assigned to each lever were drawn pseudorandomly from a set of blocks
463 with paired probabilities [block1(neutral): (0.45 0.45), block2(low contrast): (0.6 0.3),
464 block3(high contrast): (0.8 0.1)] (Fig. 1F). Note that each block type had a distinct
465 probability contrast (block1, 1:1; block2, 2:1; block3, 8:1), while maintaining the same
466 averaged reward probability (0.45), and that the outcome uncertainty within a block varied
467 with the degree of probability contrast across the two levers. The lever outcome
468 contingencies were randomly reversed to one of the three blocks every 15-30 trials,
469 except when an animal made four or more consecutive incorrect choices within certain
470 trial blocks (block2: 60:30 or block3: 80-10); such trials were excluded from trial progress.
471 When switching blocks, the transition rules imposed two restrictions: 1) the position of the
472 lever with the highest reward probability should not be the same in two consecutive blocks
473 even if the reward probability contrast changes, and 2) Neutral blocks (block1) should not
474 be repeated. Block transitions were categorized into three types based on the relative
475 cognitive challenge level before and after each block transition. If the relative challenge

476 was lower in the post-reversal block compared with the pre-reversal block, this was
477 termed a 'Hi-Lo' transition (i.e., block2→block3, block1→block2, or block1→block3). If the
478 relative uncertainty was higher in the post-reversal block compared with the pre-reversal
479 block, this was termed a 'Lo-Hi' transition (i.e., block3→block2, or block2→block1, or
480 block3→block1). If the relatively uncertainly was the same in the post-reversal block
481 compared with the pre-reversal block while still shifting probabilities across the right and
482 left levers, this was termed a 'Same' transition (i.e., block2→block2 or block3→block3)
483 (Figure S2A). In addition, in this task, during non-neutral block (i.e., blocks 1 and 3) in 40%
484 of the trials after the first 12 trials after the reversal, we probed the animal's response to
485 unexpected changes in reward size by doubling or halving the reward size (66 or 16.5 μl)
486 compared to the remaining 60% of the trials. However, the probability of win-stay, latency
487 of trial initiation, and action selection reaction time were not significantly modulated by
488 reward size (Figure S13); thus, we will not focus on this feature in this manuscript. Rats
489 were trained on the final dynaPRL task for at least 10 sessions prior to surgery.

490 **Electrode implantation**

491 All rats were surgically implanted with custom-made drivable electrode arrays, with
492 custom-designed 3D-printed pieces, sixteen insulated tungsten wires (50 um, A-M
493 Systems), and two silver ground wires, soldered to two Plexon headstage connectors
494 (Plexon Inc. TX) using standard stereotaxic procedures. Electrode arrays were placed
495 unilaterally in the left or right DMS (AP: -0.1 mm; ML: 2.45 mm; DV: -4.7 mm from Bregma).

496 **Recording and Spike sorting**

497 Following 1 week of recovery, rats were trained on the dynaPRL task again until
498 they became accustomed to performing the task while their headstage was connected

499 via a patch cable to the commutator located in the center of the chamber ceiling. Once
500 their completed trials/session reached at least 80% of their pre-surgery averaged number
501 of trials in a session (3-7 sessions), recording sessions began. Electrical signals and
502 behavioral events were collected using Plexon multichannel neural recording systems
503 (MAP system;) or Plexon OmniPlex systems, with a 40 kHz sampling rate. Neural
504 recordings at the same depth in the DMS were obtained for multiple sessions; if multiple
505 sessions from the exact recording location were included in the following analysis, the
506 data from the same channel was included only once. After that, electrodes were lowered
507 by approximately 160 μm, and recording resumed in the new location at least one day
508 later.

509 Individual units were isolated offline using principal component analysis in Offline
510 Sorter (Plexon) as described previously[92, 119-121]. Auto-correlograms, cross-correlograms,
511 the distribution of inter-spike intervals, L-ratio, and isolation distance were used to ensure
512 good isolation of single units. Spike and behavioral event timestamps were exported to
513 MATLAB (MathWorks) using customized scripts for further analysis.

514

515 **Data Analysis and Statistics**

516 **Behavioral metrics**

517 *Reversal performance*

518 Reversal performance was assessed by the probability of maintaining the same choice
519 before the contingency change, denoted as *p(perseveration)*. *p(perseveration)* was
520 computed for each trial during the last 5 trials before and the first 12 trials after the
521 contingency change. The *p(preservation)* was computed by the ratio of correct choices

522 and the total number of blocks, except that if the pre-reversal block was a neutral block,
523 in which neither side is correct, then a random side was selected as a pseudo-correct
524 choice for the calculation. A single exponential decay function was fitted to the
525 p(preservation) for the 1-12 trials after the contingency change,

526 $$p = d + a \times e^{-\lambda \times t},$$

527 where *d*, *a*, and λ represent the pre-reversal asymptotic value, the magnitude of change
528 in *p(perseveration)* after the reversal, and the learning speed, respectively. The single
529 exponential decay function was defined by MATLAB function *fittype* and curve fitting
530 employed MATLAB function *fit* with lower boundary (0, 0.5, 0) and upper boundary (3, 2,
531 1) for parameters d, a, and λ correspondingly. Averaged parameter values across 9
532 iterations were used for each subject and session.

533 *Matching performance, stay probabilities, and latencies*

534 To assess how animals allocate their responses (left and right lever presses) to the local
535 (within a block) reward probabilities of each choice option after the learning period (first
536 12 trials), we calculated the *matching score*[50] as a deviation of left response probability,
537 *p(left),* from the reward probability given select the left choice, *p(reward|choice=left)*.
538 Deviation < 0 is undermatching, and > 0 is overmatching.

539 We measured the overall stay probability by calculating the likelihood of repeating the
540 same choice as the last trial. Then, conditional stay probabilities were also calculated
541 separately for the reward or unrewarded outcome in the last trial and denoted as
542 *p(stay|win)* and *p(stay|lose)* correspondingly. The difference between win-stay and lose-
543 shift was measured by ΔWSLS = *p(stay|win) – p(shift|lose)*.

544 The latencies (response times) measured the time interval between stimulus (center light
545 illumination or lever insertion) and response or reaction (magazine entry or lever press)
546 to that stimulus. As the distribution of latencies is highly skewed to the left (zero), a natural
547 logarithm transformation was used to make the distribution of latencies more akin to
548 normal distribution.

549 **Classification analysis**

550 *Support vector machine (SVM)*

551 SVM was employed to decode group membership (CIE vs. Air), sex label (male vs.
552 female), and assessment phase (only for PRL task, pre-vapor vs. post-vapor) from the
553 behavior dataset. SVM modeling was performed using the MATLAB function *fitclinear* for
554 the classification of binary group membership and *fitecoc* for the classification of multi-
555 subject labels. For both classification approaches, we used a total of 20 behavioral
556 measures (columns) from each session consisting of reversal decay in post-reversal and
557 matching score in pre-reversal, as well as 9 other behavioral measurements in pre- and
558 post-block transitions, accordingly. The behavior dataset was randomly divided into two
559 parts into a training set and a test set with a 90:10 ratio. Within the training set, a linear
560 SVM model was optimized using 10-fold cross-validation. This approach involves dividing
561 the training set into 10 equal parts, training the model on nine parts, and validating it on
562 the tenth part. This process is repeated ten times, with each part used once as the
563 validation set. The results from these iterations are used to fine-tune the model
564 parameters. The optimized SVM model was then evaluated on a test set to assess its
565 generalizability and predictive performance. This train-test process was repeated 1000
566 times. True positive (TP), true negative (TN), false positive (FP, type I error), and false

negative (FN, type II error) were calculated based on actual predicted data labels. For the multilabel classification, precision [TP/(TP+FP)] was used to assess model performance in predicting each class. To determine whether the observed decoding accuracy for group membership and sex label was significantly higher than what would be expected by chance, we conducted Monte Carlo significance tests, and the p-value was computed as follows:

p = [Number of iterations ($\text{Precisions}^{\text{Data}} < \text{Precisions}^{\text{Shuffle}}$) + 1]/(Total number of iterations + 1)

Uniform manifold approximation and projection (UMAP)

The manifold learning technique, UMAP, was employed to perform non-linear dimensional reduction of our behavior data matrix from above. We used the UMAP implementation provided in the MATLAB community *UMAP*[122].

Reinforcement learning models

Reinforcement learning (RL) models assume that choices stem from the cumulative outcomes of actions accrued over numerous trials. We fitted the choice and outcome data to eight distinct RL models: 1, standard Q-learning model; 2, Q-learning model with differential learning rates (Q-DFLr); 3, differential forgetting RL model (DF-RL); 4, DF-RL model with inverse temperature β (DF-RLwβ); 5, forgetting RL model (F-RL); 6, F-RL model with inverse temperature β (F-RLwβ); 7, win-stay lose-shift model (WSLS); 8, biased random choice model (RD).

For models 1 through 4, choices are assumed to follow learned values for each option, Q, according to softmax function, in which the probability of choice k on trial t is:

$$P_k(t) = \frac{e^{\beta Q_k(t)}}{\sum_{i=1}^{k} e^{\beta Q_k(t)}}$$

Here, β is the inverse temperature parameter that controls the level of stochasticity in the choice, with β=0 resulting in equal probability over all choice options. β was set to a constant 1 for models 4 and 6.

The value updating for each model is described below:

Model 1: Q-learning model,

If *c*(*t*) = L,

$$Q_L(t+1) = Q_L(t) + \alpha\big(\mathrm{r(t)} - Q_L(t)\big)$$

$$Q_R(t+1) = Q_R(t)$$

, where *c*(*t*) is the choice side (left, L or right, R) in the current trial, *r*(*t*) is the outcome on that trial, and α, the learning rate, controls the update of the chosen action value according to the reward prediction error $r(t) - Q_L(t)$.

Model 2: Q-learning model with differential learning rates (Q-DFLr),

If *c*(t) = L and *r*(t) = 1,

$$Q_L(t+1) = Q_L(t) + \alpha^{+}\big(\mathrm{r(t)} - Q_L(t)\big)$$

$$Q_R(t+1) = (1 - \theta^{+})\, Q_R(t)$$

If *c*(t) = L and *r*(t) = 0,

$$Q_L(t+1) = Q_L(t) + \alpha^{-}\big(\mathrm{r(t)} - Q_L(t)\big)$$

$$Q_R(t+1) = (1 - \theta^-)\, Q_R(t)$$

Here, value updates are governed by different learning rates for positive, α^+, or omitted, α^-, outcomes and the non-chosen option is decay by a forgetting rate, θ^+ or θ^-, for rewarded and unrewarded trials respectively.

Model 3 and 4: Differential forgetting RL (DF-RL) and DF-RL with (model 4) or without (model 3) free β,

If *c*(t) = L and *r*(t) = 1,

$$Q_L(t+1) = \gamma_c Q_L(t) + k^+$$

$$Q_R(t+1) = \gamma_{uc} Q_R(t)$$

If *c*(t) = L and *r*(t) = 0,

$$Q_L(t+1) = \gamma_c Q_L(t) + k^-$$

$$Q_R(t+1) = \gamma_{uc} Q_R(t)$$

where κ^+ and κ^- directly update the chosen action value in rewarded and unrewarded trials, respectively. γ_c and γ_{uc} are the forgetting factor in updating chosen and unchosen action values, respectively. Accordingly, forgetting rates θ_c and θ_{uc} in models 3 and 4 corresponds to 1-γ_c and 1-γ_{uc}, respectively.

Model 5 and 6: Forgetting RL models (F-RL) and F-RL with (model 6) or without (model 5) free β,

If *c*(t) = L and *r*(t) = 1,

$$Q_L(t+1) = \gamma Q_L(t) + k^+$$

If *c*(t) = L and *r*(t) = 0,

$$Q_L(t+1) = \gamma Q_L(t) + k^-$$

For the unchosen right side,

$$Q_R(t+1) = \gamma Q_R(t)$$

where κ^+ and κ^- directly update the chosen action value in rewarded and unrewarded trials, respectively. γ is the forgetting factor in updating chosen and unchosen action values.

Models 7 and 8 directly describe the probability of each choice option on trial t, either subject to experienced outcomes (WSLS) or as a fixed proportion of choice.

Model 7: Win-stay lose-shift.

If *c*(t) = L and *r*(t) = 1,

$$P_L(t+1) = 1 - \epsilon/2$$

$$P_R(t+1) = \epsilon/2$$

If *c*(t) = L and *r*(t) = 0,

$$P_L(t+1) = \epsilon/2$$

$$P_R(t+1) = 1 - \epsilon/2$$

Where ϵ controls the randomness of the stay probability.

Model 8: Biased random choice.

$$P_L(t+1) = \varphi$$

$$P_R(t+1) = 1 - \varphi$$

Where φ controls the bias of choice probability.

Hierarchical model fitting and model comparisons

We used the Matlab Stan interface (https://mc-stan.org/users/interfaces/matlab-stan) to construct and sample from hierarchical RL models, in which group-level hyperparameters govern individual rat parameters, to avoid overfitting to inter-rat noise [123]. For a given model, we used Stan to draw consecutive samples from the posterior density of the model parameters using Hamiltonian Markov chain Monte Carlo (HMC), giving density estimates for the best fitting model parameters for the aggregate choice and outcome data across all sessions and rats. For each model, rat-level parameters were drawn from a group-level distribution with group mean, μ, group mean difference, δ, and variance σ. To quantify the evidence of group differences, the Directed Bayes Factor (dBF) was employed. This measure calculates the ratio of the proportion of the distribution of δ (group difference) that is above zero to the proportion that is below zero as in[115]. Given the difficulties in sampling from hierarchical RL models, parameters were transformed such that sample were drawn in an unconstrained space and later transformed into bounded values using the fast approximation of the cumulative normal distribution function, *phi_approx*[124]. We set normally distributed priors for all parameters at the rat level: N(0, 1) for all parameters, except β, which was set at N(0, 10), while group-level hyperparameters were given a prior normal prior distribution of N(0, 2) for μ and δ; and a gamma distribution of (2, 0.5) for σ. Hierarchical models for each of the candidate RL models were sampled for 2,000 iterations after 1,000 warm-up draws for four chains in parallel. All other settings adhered to the default configuration.

669 Predictive accuracy of each model was estimated using leave-one-out cross
670 validation with Pareto-smoothed importance sampling (psis-loo) using the model log
671 likelihood computed for each of the sampled parameters on the actual choice and
672 outcome data[125]. For simulations of behavior, we took the mean of the posterior samples
673 (i.e. over the 2000 post-warm up draws) for each rat-level model parameter as the best-
674 fitting estimate for that individual subject. Using these best-fitting model parameters, we
675 simulated choice behavior on the actual task structure. A reversal analysis, analogous to
676 the one used on the empirical data, was applied to these simulated data to probe whether
677 the model could recapitulate the key differences in choice behavior observed in the
678 empirical data.

679 **Multiple linear regression**

680 To examine how neural spike activity was modulated by different behavioral and decision
681 variables, we employed multiple linear regression models to fit spike rates of each unit as
682 a linear function of various factors, such as rat's choice, reward outcome, and estimated
683 action values as in[32, 52]. All trials in each session other than those with choice omission
684 were included in the analysis. To investigate the evolution of neural spike modulation
685 within a temporal window surrounding key behavioral events, including lever insertion,
686 action selection, and outcome presentation, we aligned the spikes of each neuron to the
687 onset of these behavioral events. We then quantified the firing rates of each neuron using
688 a sliding time bin approach. Specifically, we employed a 100-ms time bin with 50-ms steps
689 or a 200-ms time bin with 100-ms steps. This analysis was conducted within predefined
690 temporal windows relative to trial initiation, lever insertion, lever press, and outcome,
691 presentation, which were set at -700 ms to 300 ms, -500 ms to 500 ms, -500 ms to 500

692 ms, and -100 ms to 1000 ms, respectively. To control for the temporal auto-correlation
693 among spikes[126], we added auto-regression (AR) terms as in Shin et al.[52] for all of the
694 following regression models. To investigate the influence of both current and preceding
695 choices, outcomes, and their interaction on the spike activity of individual neurons, we
696 employed a regression model to delineate the firing rate (*S*) as a function of choice
697 direction (*C*; ipsi or contra-lateral to implant side), outcome (*O*; rewarded or unrewarded),
698 and their interaction (*I*) in current trial *t* and last trial *t*-1, along with autoregressive
699 components (*AR*), as the following

700 $S(t) = \beta_0 + \beta_1 \times C(t) + \beta_2 \times C(t-1) + \beta_3 \times O(t) + \beta_4 \times O(t-1) + \beta_5 \times I(t) + \beta_6 \times$
701 $I(t-1) + AR + \varepsilon(t)$,

702 where β_0 through β_6 represent standardized regression coefficients, and the error term is
703 $\epsilon(t)$. AR term was defined as follows:

704 $AR = \beta_7 \times S(t-1) + \beta_8 \times S(t-2) + \beta_9 \times S(t-3)$,

705 To examine how chosen value-related signals are represented by neurons at the time
706 that choice and outcome are revealed, we used the following regression:

707 $S(t) = \beta_0 + \beta_1 \times C(t) + \beta_2 \times O(t) + \beta_3 \times I(t) + \beta_4 \times Q_c(t) + AR + \varepsilon(t)$,

708 where Q_c is the chosen value estimated by the best fit RL model.

709 To investigate how different types of value signals are encoded in neuronal activity, we
710 used a regression model as follows:

711 $S(t) = \beta_0 + \beta_1 \times C(t) + \beta_2 \times \Sigma Q(t) + \beta_3 \times \Delta Q(t) + \beta_4 \times Q_c(t) + AR + \varepsilon(t)$,

712 where $\Sigma Q(t) = Q_{ipsi}(t) + Q_{contra}(t)$ and $\Delta Q(t) = Q_{ipsi}(t) - Q_{contra}(t)$, which can
713 approximate state value and policy, respectively[32, 52].

714 To capture the main variance of the coefficient across time bins, we ran a PCA on
715 standardized regression coefficients. The magnitude of PC1 scores were used as a proxy
716 of the overall modulation effect of decision factors on firing during the time window aligned
717 to lever insertion, lever pressing, and outcome presentation.

718 **Generalized linear mixed-effect models (GLMMs)**

719 To understand the impact of EtOH treatment on the proportion of neural responses to
720 specific decision variables described above, we employ a Generalized Linear Mixed-
721 Effects Model (GLMM) to account for the random effects associated with individual
722 animals and specific neurons within those animals. The model is described by the
723 following Wikison notation:

724 *Response_Significance* ~ *Group* + (*1*|*AnimalID*) + (*1*|*AnimalID*:*NeuronID*),

725 Where *Response_Significance* denotes the binary variable (e.g., significantly or not
726 modulated) derived from the preceding multiple linear regression, and *Group* represents
727 a fixed effect, such as an EtOH or Air group. The random effects are specified as
728 *1*|*AnimalID* and *1*|*AnimalID*:*NeuronID*. The term *1*|*AnimalID* introduces a random
729 intercept for each animal, allowing for the acknowledgment of variability in baseline
730 response levels across animals. The term *1*|*AnimalID:NeuronID* adds another layer of
731 random intercepts, this time to account for variability at the neuron level within each
732 animal, acknowledging that responses may differ not just between animals but also

among neurons within the same animal. To fit this model, we utilize the *fitglme* function in MATLAB with a 'Binomial' distribution and a 'Logit' link function.

To assess the influence of EtOH treatment on the overall modulational strength attributed to decision variables, we applied the following GLMM,

PC1score ~ *Group* + (*1*|*AnimalID*)

Here, *PC1score* represents the aggregate modulation effect derived from PCA on coefficients obtained from the aforementioned multiple linear regression analysis. This model was estimated using the *fitlme* function in MATLAB.

The p-value of the *Group* coefficient denotes the main effect of EtOH treatment.

Other statistical analysis

Behavioral data were analyzed using paired *t*-tests, one-way ANOVA with repeated measures (one-way RM ANOVA), or mixed effect ANOVA (also known as two-way ANOVA with repeated measures, two-way RM ANOVA) followed by Bonferroni *post hoc* test, all conducted in MATLAB. A p-value < 0.05 was used as the criterion to determine statistical significance unless noted otherwise. All data are expressed as the mean ± standard error of the mean.

750 **Data availability**

751 The datasets generated for this manuscript are available on request to
752 ycheng62@jhu.edu and patricia.janak@jhu.edu. The code used in this manuscript is
753 availble on github https://github.com/cyf203/CIE_flexibility_DMSrecording upon the
754 publicaiton.

755

756 **Ethics statement**

757 All animal care and experimental procedures were approved by the Johns Hopkins
758 University Institutional Animal Care and Use Committee and were conducted in
759 accordance with the *National Research Council Guide for the Care and Use of Laboratory*
760 *Animals*.

761

762

763 **Author contributions**

764 Conceptualization: YC and PHJ. Reinforcement learning modeling: YC and AL. Analysis
765 design on electrophysiology data: YC and DL. Other methodology, formal analysis and
766 visualization: YC. Experiments and designs: YC and RM. Writing and discussion: YC,
767 RM, AL, DL and PHJ. Supervision and funding: PHJ.

768 **FUNDING**

769 This research was supported by R01AA026306 (PHJ) and R01DA035943 (PHJ).

770 **References**

771 1. Barker, J.M., Corbit, L.H., *et al.* Corticostriatal circuitry and habitual ethanol
772 seeking. *Alcohol* **49**, 817-824 (2015).

773 2. Corbit, L.H. & Janak, P.H. Habitual Alcohol Seeking: Neural Bases and Possible
774 Relations to Alcohol Use Disorders. *Alcohol Clin Exp Res* **40**, 1380-1389 (2016).

775 3. Renteria, R., Baltz, E.T. & Gremel, C.M. Chronic alcohol exposure disrupts top-
776 down control over basal ganglia action selection to produce habits. *Nat Commun* **9**, 211
777 (2018).

778 4. Sjoerds, Z., de Wit, S., *et al.* Behavioral and neuroimaging evidence for
779 overreliance on habit learning in alcohol-dependent patients. *Transl Psychiatry* **3**, e337
780 (2013).

781 5. Sebold, M., Deserno, L., *et al.* Model-based and model-free decisions in alcohol
782 dependence. *Neuropsychobiology* **70**, 122-131 (2014).

783 6. Shields, C.N. & Gremel, C.M. Prior Chronic Alcohol Exposure Enhances
784 Pavlovian-to-Instrumental Transfer. *Alcohol* (2021).

785 7. Corbit, L.H., Nie, H. & Janak, P.H. Habitual responding for alcohol depends upon
786 both AMPA and D2 receptor signaling in the dorsolateral striatum. *Front Behav Neurosci*
787 **8**, 301 (2014).

788 8. Groman, S.M., Hillmer, A.T., *et al.* Midbrain D3 Receptor Availability Predicts
789 Escalation in Cocaine Self-administration. *Biol Psychiatry* **88**, 767-776 (2020).

790 9. Istin, M., Thiriet, N. & Solinas, M. Behavioral flexibility predicts increased ability to
791 resist excessive methamphetamine self-administration. *Addict Biol* **22**, 958-966 (2017).

792 10. Villiamma, P., Casby, J. & Groman, S.M. Adolescent reinforcement-learning
793 trajectories predict cocaine-taking behaviors in adult male and female rats.
794 *Psychopharmacology* **239**, 2885-2901 (2022).
795 11. Turyabahika-Thyen, K. & Wolffgramm, J. Loss of flexibility in alcohol-taking rats:
796 promoting factors. *Eur Addict Res* **12**, 210-221 (2006).
797 12. Rodberg, E.M. & Vazey, E.M. Individual differences in behavioral flexibility predict
798 future volitional ethanol consumption in mice. *Alcohol* **101**, 37-43 (2022).
799 13. De Falco, E., White, S.M.*, et al.* Impaired cognitive flexibility and heightened
800 urgency are associated with increased alcohol consumption in rodent models of
801 excessive drinking. *Addict Biol* **26**, e13004 (2021).
802 14. Shnitko, T.A., Gonzales, S.W. & Grant, K.A. Low cognitive flexibility as a risk for
803 heavy alcohol drinking in non-human primates. *Alcohol* **74**, 95-104 (2019).
804 15. Czapla, M., Simon, J.J.*, et al.* The impact of cognitive impairment and impulsivity
805 on relapse of alcohol-dependent patients: implications for psychotherapeutic treatment.
806 *Addict Biol* **21**, 873-884 (2016).
807 16. Maillard, A., Laniepce, A.*, et al.* Prognostic factors for low‐risk drinking and
808 relapse in alcohol use disorder: A multimodal analysis. *Addict Biol* **27** (2022).
809 17. Izquierdo, A. & Jentsch, J.D. Reversal learning as a measure of impulsive and
810 compulsive behavior in addictions. *Psychopharmacology* **219**, 607-620 (2012).
811 18. Ghods-Sharifi, S., Haluk, D.M. & Floresco, S.B. Differential effects of inactivation
812 of the orbitofrontal cortex on strategy set-shifting and reversal learning. *Neurobiol. Learn.*
813 *Mem.* **89**, 567-573 (2008).

814 19. Reiter, A.M., Deserno, L.*, et al.* Behavioral and Neural Signatures of Reduced
815 Updating of Alternative Options in Alcohol-Dependent Patients during Flexible Decision-
816 Making. *J Neurosci* **36**, 10935-10948 (2016).
817 20. Chanraud, S., Reynaud, M.*, et al.* Diffusion Tensor Tractography in Mesencephalic
818 Bundles: Relation to Mental Flexibility in Detoxified Alcohol-Dependent Subjects.
819 *Neuropsychopharmacology : official publication of the American College of*
820 *Neuropsychopharmacology* **34**, 1223-1232 (2009).
821 21. Jokisch, D., Roser, P., Juckel, G., Daum, I. & Bellebaum, C. Impairments in
822 learning by monetary rewards and alcohol-associated rewards in detoxified alcoholic
823 patients. *Alcohol Clin Exp Res* **38**, 1947-1954 (2014).
824 22. Mason, B.J. Emerging pharmacotherapies for alcohol use disorder.
825 *Neuropharmacology* **122**, 244-253 (2017).
826 23. Macht, V., Elchert, N. & Crews, F. Adolescent Alcohol Exposure Produces
827 Protracted Cognitive-Behavioral Impairments in Adult Male and Female Rats. *Brain*
828 *Sciences* **10**, 785 (2020).
829 24. Dannenhoffer, C.A., Robertson, M.M.*, et al.* Chronic alcohol exposure during
830 critical developmental periods differentially impacts persistence of deficits in cognitive
831 flexibility and related circuitry. *International Review of Neurobiology* **160**, 117-173 (2021).
832 25. Badanich, K.A., Becker, H.C. & Woodward, J.J. Effects of chronic intermittent
833 ethanol exposure on orbitofrontal and medial prefrontal cortex-dependent behaviors in
834 mice. *Behav Neurosci* **125**, 879-891 (2011).
835 26. Kroener, S., Mulholland, P.J.*, et al.* Chronic Alcohol Exposure Alters Behavioral
836 and Synaptic Plasticity of the Rodent Prefrontal Cortex. *PloS one* **7**, e37541 (2012).

837 27. Kuzmin, A., Liljequist, S., *et al.* Repeated moderate-dose ethanol bouts impair
838 cognitive function in Wistar rats. *Addict Biol* **17**, 132-140 (2012).
839 28. Ho, A.M.-C., Peyton, M.P., *et al.* Chronic Intermittent Ethanol Exposure Alters
840 Behavioral Flexibility in Aged Rats Compared to Adult Rats and Modifies Protein and
841 Protein Pathways Related to Alzheimer's Disease. *ACS Omega* **7**, 46260-46276 (2022).
842 29. Pickens, C.L., Gallo, M., Fisher, H., Pajser, A. & Ray, M.H. Alcohol Consumption
843 during Adulthood Does Not Impair Later Go/No-Go Reversal Learning in Male Rats.
844 *NeuroSci* **2**, 166-176 (2021).
845 30. Aguirre, C.G., Stolyarova, A., *et al.* Sex-dependent effects of chronic intermittent
846 voluntary alcohol consumption on attentional, not motivational, measures during
847 probabilistic learning and reversal. *PloS one* **15**, e0234729 (2020).
848 31. Ray, M.H., Hite, T., Gallo, M. & Pickens, C.L. Operant over-responding is more
849 sensitive than reversal learning for revealing behavioral changes after withdrawal from
850 alcohol consumption. *Physiol Behav* **196**, 176-184 (2018).
851 32. Kim, H., Sul, J.H., Huh, N., Lee, D. & Jung, M.W. Role of striatum in updating
852 values of chosen actions. *J Neurosci* **29**, 14701-14712 (2009).
853 33. Izquierdo, A., Brigman, J.L., Radke, A.K., Rudebeck, P.H. & Holmes, A. The neural
854 basis of reversal learning: An updated perspective. *Neuroscience* **345**, 12-26 (2017).
855 34. Wang, J., Cheng, Y., *et al.* Alcohol elicits functional and structural plasticity
856 selectively in dopamine D1 receptor-expressing neurons of the dorsomedial striatum. *J*
857 *Neurosci* **35**, 11634-11643 (2015).
858 35. Cheng, Y., Huang, C.C.Y., *et al.* Distinct synaptic strengthening of the striatal direct
859 and indirect pathways drives alcohol consumption. *Biol Psychiatry* **81**, 918-929 (2017).

860 36. Cheng, Y., Wang, X.*, et al.* Prenatal Exposure to Alcohol Induces Functional and
861 Structural Plasticity in Dopamine D1 Receptor-Expressing Neurons of the Dorsomedial
862 Striatum. *Alcohol Clin Exp Res* **42**, 1493-1502 (2018).
863 37. Cheng, Y., Xie, X.*, et al.* Optogenetic induction of orbitostriatal long-term
864 potentiation in the dorsomedial striatum elicits a persistent reduction of alcohol-seeking
865 behavior in rats. *Neuropharmacology* **191**, 108560 (2021).
866 38. Ma, T., Cheng, Y.*, et al.* Bidirectional and long-lasting control of alcohol-seeking
867 behavior by corticostriatal LTP and LTD. *Nat Neurosci* **21**, 373-383 (2018).
868 39. Lu, J., Cheng, Y.*, et al.* Alcohol intake enhances glutamatergic transmission from
869 D2 receptor-expressing afferents onto D1 receptor-expressing medium spiny neurons in
870 the dorsomedial striatum. *Neuropsychopharmacology : official publication of the*
871 *American College of Neuropsychopharmacology* **44**, 1123-1131 (2019).
872 40. Ma, T., Huang, Z.*, et al.* Chronic alcohol drinking persistently suppresses
873 thalamostriatal excitation of cholinergic neurons to impair cognitive flexibility. *Journal of*
874 *Clinical Investigation* **132** (2021).
875 41. Tai, L.H., Lee, A.M., Benavidez, N., Bonci, A. & Wilbrecht, L. Transient stimulation
876 of distinct subpopulations of striatal neurons mimics changes in action value. *Nat*
877 *Neurosci* **15**, 1281-1289 (2012).
878 42. Parker, N.F., Cameron, C.M.*, et al.* Reward and choice encoding in terminals of
879 midbrain dopamine neurons depends on striatal target. *Nat Neurosci* **19**, 845-854 (2016).
880 43. Trantham-Davidson, H., Burnett, E.J.*, et al.* Chronic alcohol disrupts dopamine
881 receptor activity and the cognitive function of the medial prefrontal cortex. *J Neurosci* **34**,
882 3706-3718 (2014).

883 44. Gilpin, N.W., Smith, A.D., *et al.* Operant behavior and alcohol levels in blood and
884 brain of alcohol-dependent rats. *Alcohol Clin Exp Res* **33**, 2113-2123 (2009).
885 45. Bi, J., Sun, J., Wu, Y., Tennen, H. & Armeli, S. A machine learning approach to
886 college drinking prediction and risk factor identification. *ACM Transactions on Intelligent*
887 *Systems and Technology* **4**, 1-24 (2013).
888 46. Whelan, R., Watts, R., *et al.* Neuropsychosocial profiles of current and future
889 adolescent alcohol misusers. *Nature* **512**, 185-189 (2014).
890 47. Kinreich, S., Meyers, J.L., *et al.* Predicting risk for Alcohol Use Disorder using
891 longitudinal data with multimodal biomarkers and family history: a machine learning study.
892 *Mol. Psychiatry* **26**, 1133-1141 (2021).
893 48. Grossman, C.D., Bari, B.A. & Cohen, J.Y. Serotonin neurons modulate learning
894 rate through uncertainty. *Curr Biol* **32**, 586-599 e587 (2021).
895 49. Funamizu, A., Ito, M., Doya, K., Kanzaki, R. & Takahashi, H. Uncertainty in
896 action - value estimation affects both action choice and learning rate of the choice
897 behaviors of rats. *European Journal of Neuroscience* **35**, 1180-1189 (2012).
898 50. Trepka, E., Spitmaan, M., *et al.* Entropy-based metrics for predicting choice
899 behavior based on local response to reward. *Nat Commun* **12**, 6567 (2021).
900 51. Iigaya, K., Ahmadian, Y., *et al.* Deviation from the matching law reflects an optimal
901 strategy involving learning over multiple timescales. *Nat Commun* **10** (2019).
902 52. Shin, E.J., Jang, Y., *et al.* Robust and distributed neural representation of action
903 values. *eLife* **10** (2021).

904 53. Ridenour, T.A., Cottler, L.B., Compton, W.M., Spitznagel, E.L. & Cunningham-
905 Williams, R.M. Is there a progression from abuse disorders to dependence disorders?
906 *Addiction* **98**, 635-644 (2003).
907 54. Manning, V., Wanigaratne, S.*, et al.* Changes in Neuropsychological Functioning
908 during Alcohol Detoxification. *Eur Addict Res* **14**, 226-233 (2008).
909 55. Loeber, S., Duka, T.*, et al.* Effects of Repeated Withdrawal from Alcohol on
910 Recovery of Cognitive Impairment under Abstinence and Rate of Relapse. *Alcohol and*
911 *alcoholism* **45**, 541-547 (2010).
912 56. Moselhy, H.F. FRONTAL LOBE CHANGES IN ALCOHOLISM: A REVIEW OF
913 THE LITERATURE. *Alcohol and alcoholism* **36**, 357-368 (2001).
914 57. Chanraud, S., Martelli, C.*, et al.* Brain Morphometry and Cognitive Performance in
915 Detoxified Alcohol-Dependents with Preserved Psychosocial Functioning.
916 *Neuropsychopharmacology : official publication of the American College of*
917 *Neuropsychopharmacology* **32**, 429-438 (2007).
918 58. Oscar-Berman, M., Shagrin, B., Evert, D.L. & Epstein, C. Impairments of brain and
919 behavior: the neurological effects of alcohol. *Alcohol Health Res World* **21**, 65-75 (1997).
920 59. Schulte, T., Müller-Oehring, E.M., Salo, R., Pfefferbaum, A. & Sullivan, E.V.
921 Callosal involvement in a lateralized stroop task in alcoholic and healthy subjects.
922 *Neuropsychology* **20**, 727-736 (2006).
923 60. Pfefferbaum, A., Sullivan, E.V.*, et al.* In vivo detection and functional correlates of
924 white matter microstructural disruption in chronic alcoholism. *Alcohol Clin Exp Res* **24**,
925 1214-1221 (2000).

926 61. Duka, T., Townshend, J.M., Collier, K. & Stephens, D.N. Impairment in cognitive
927 functions after multiple detoxifications in alcoholic inpatients. *Alcohol Clin Exp Res* **27**,
928 1563-1572 (2003).
929 62. Vanes, L.D., Holst, R.J.*, et al.* Contingency Learning in Alcohol Dependence and
930 Pathological Gambling: Learning and Unlearning Reward Contingencies. *Alcohol Clin*
931 *Exp Res* **38**, 1602-1610 (2014).
932 63. Corbit, L.H., Nie, H. & Janak, P.H. Habitual alcohol seeking: time course and the
933 contribution of subregions of the dorsal striatum. *Biol Psychiatry* **72**, 389-395 (2012).
934 64. Dominguez, G., Belzung, C.*, et al.* Alcohol withdrawal induces long-lasting spatial
935 working memory impairments: relationship with changes in corticosterone response in the
936 prefrontal cortex. *Addict Biol* **22**, 898-910 (2017).
937 65. Shnitko, T.A., Gonzales, S.W., Newman, N. & Grant, K.A. Behavioral Flexibility in
938 Alcohol‐Drinking Monkeys: The Morning After. *Alcohol Clin Exp Res* **44**, 729-737 (2020).
939 66. Castillo-Carniglia, A., Keyes, K.M., Hasin, D.S. & Cerdá, M. Psychiatric
940 comorbidities in alcohol use disorder. *The Lancet Psychiatry* **6**, 1068-1080 (2019).
941 67. Birrell, J.M. & Brown, V.J. Medial Frontal Cortex Mediates Perceptual Attentional
942 Set Shifting in the Rat. *J Neurosci* **20**, 4320-4324 (2000).
943 68. Gangal, H., Xie, X.*, et al.* Drug Reinforcement Impairs Cognitive Flexibility by
944 Inhibiting Striatal Cholinergic Neurons. (Cold Spring Harbor Laboratory, 2022).
945 69. Bağci, B., Düsmez, S.*, et al.* Computational analysis of probabilistic reversal
946 learning deficits in male subjects with alcohol use disorder. *Frontiers in psychiatry* **13**
947 (2022).

948 70. Morris, L.S., Baek, K.*, et al.* Biases in the Explore–Exploit Tradeoff in Addictions:
949 The Role of Avoidance of Uncertainty. *Neuropsychopharmacology : official publication of*
950 *the American College of Neuropsychopharmacology* **41**, 940-948 (2016).
951 71. Cockburn, J., Man, V., Cunningham, W.A. & O'Doherty, J.P. Novelty and
952 uncertainty regulate the balance between exploration and exploitation through distinct
953 mechanisms in the human brain. *Neuron* **110**, 2691-2702.e2698 (2022).
954 72. Gershman, S.J. Uncertainty and Exploration. *Decision (Wash D C)* **6**, 277-286
955 (2019).
956 73. Bechara, A., Dolan, S.*, et al.* Decision-making deficits, linked to a dysfunctional
957 ventromedial prefrontal cortex, revealed in alcohol and stimulant abusers.
958 *Neuropsychologia* **39**, 376-389 (2001).
959 74. Goudriaan, A.E., Oosterlaan, J., de Beurs, E. & van den Brink, W. Decision making
960 in pathological gambling: A comparison between pathological gamblers, alcohol
961 dependents, persons with Tourette syndrome, and normal controls. *Cognitive Brain*
962 *Research* **23**, 137-151 (2005).
963 75. Oglesby, M.E., Albanese, B.J., Chavarria, J. & Schmidt, N.B. Intolerance of
964 Uncertainty in Relation to Motives for Alcohol Use. *Cognitive Therapy and Research* **39**,
965 356-365 (2015).
966 76. Koob, G.F., Powell, P. & White, A. Addiction as a Coping Response: Hyperkatifeia,
967 Deaths of Despair, and COVID-19. *American Journal of Psychiatry* **177**, 1031-1037
968 (2020).

969 77. Oberlin, B.G. & Grahame, N.J. High-alcohol preferring mice are more impulsive
970 than low-alcohol preferring mice as measured in the delay discounting task. *Alcohol Clin*
971 *Exp Res* **33**, 1294-1303 (2009).
972 78. Perkel, J.K., Bentzley, B.S., Andrzejewski, M.E. & Martinetti, M.P. Delay
973 discounting for sucrose in alcohol-preferring and nonpreferring rats using a sipper tube
974 within-sessions task. *Alcohol Clin Exp Res* **39**, 232-238 (2015).
975 79. Smith, C.T., Steel, E.A., Parrish, M.H., Kelm, M.K. & Boettiger, C.A. Intertemporal
976 Choice Behavior in Emerging Adults and Adults: Effects of Age Interact with Alcohol Use
977 and Family History Status. *Front Hum Neurosci* **9**, 627 (2015).
978 80. Barker, J.M., Bryant, K.G., Osborne, J.I. & Chandler, L.J. Age and Sex Interact to
979 Mediate the Effects of Intermittent, High-Dose Ethanol Exposure on Behavioral Flexibility.
980 *Frontiers in pharmacology* **8**, 450 (2017).
981 81. Pratap, U.P., Patil, A.*, et al.* Estrogen-induced neuroprotective and anti-
982 inflammatory effects are dependent on the brain areas of middle-aged female rats. *Brain*
983 *Research Bulletin* **124**, 238-253 (2016).
984 82. Zhang, Q.-G., Wang, R.*, et al.* Brain-derived estrogen exerts anti-inflammatory and
985 neuroprotective actions in the rat hippocampus. *Molecular and Cellular Endocrinology*
986 **389**, 84-91 (2014).
987 83. Lei, H., Mochizuki, Y.*, et al.* Sex difference in the weighting of expected uncertainty
988 under chronic stress. *Sci Rep* **11**, 8700 (2021).
989 84. Daw, N.D., Niv, Y. & Dayan, P. Actions, policies, values and the basal ganglia. in
990 *Recent Breakthroughs in Basal Ganglia Research* (2005).

991 85. Groman, S.M., Thompson, S.L., Lee, D. & Taylor, J.R. Reinforcement learning
992 detuned in addiction: integrative and translational approaches. *Trends Neurosci* **45**, 96-
993 105 (2022).
994 86. Beylergil, S.B., Beck, A.*, et al.* Dorsolateral prefrontal cortex contributes to the
995 impaired behavioral adaptation in alcohol dependence. *Neuroimage Clin* **15**, 80-94
996 (2017).
997 87. Ito, M. & Doya, K. Validation of decision-making models and analysis of decision
998 variables in the rat basal ganglia. *J Neurosci* **29**, 9861-9874 (2009).
999 88. Samejima, K., Ueda, Y., Doya, K. & Kimura, M. Representation of action-specific
1000 reward values in the striatum. *Science* **310**, 1337-1340 (2005).
1001 89. Lau, B. & Glimcher, P.W. Value representations in the primate striatum during
1002 matching behavior. *Neuron* **58**, 451-463 (2008).
1003 90. Stalnaker, T.A., Calhoon, G.G., Ogawa, M., Roesch, M.R. & Schoenbaum, G.
1004 Neural correlates of stimulus-response and response-outcome associations in
1005 dorsolateral versus dorsomedial striatum. *Front Integr Neurosci* **4**, 12 (2010).
1006 91. Kim, H., Lee, D. & Jung, M.W. Signals for previous goal choice persist in the
1007 dorsomedial, but not dorsolateral striatum of rats. *J Neurosci* **33**, 52-63 (2013).
1008 92. Vandaele, Y., Mahajan, N.R.*, et al.* Distinct recruitment of dorsomedial and
1009 dorsolateral striatum erodes with extended training. *Elife* **8** (2019).
1010 93. Her, E.S., Huh, N., Kim, J. & Jung, M.W. Neuronal activity in dorsomedial and
1011 dorsolateral striatum under the requirement for temporal credit assignment. *Sci Rep* **6**,
1012 27056 (2016).

1013 94. Bloem, B., Huda, R.*, et al.* Multiplexed action-outcome representation by striatal
1014 striosome-matrix compartments detected with a mouse cost-benefit foraging task. *Nat*
1015 *Commun* **13** (2022).
1016 95. Nishioka, T., Macpherson, T., Hamaguchi, K. & Hikida, T. Distinct Roles of
1017 Dopamine D1 and D2 Receptor-expressing Neurons in the Nucleus Accumbens for a
1018 Strategy Dependent Decision Making. (bioRxiv, 2021).
1019 96. Bolkan, S.S., Stone, I.R.*, et al.* Opponent control of behavior by dorsomedial
1020 striatal pathways depends on task demands and internal state. *Nat Neurosci* **25**, 345-357
1021 (2022).
1022 97. Lee, J. & Sabatini, B.L. Striatal indirect pathway mediates exploration via collicular
1023 competition. *Nature* **599**, 645-649 (2021).
1024 98. Matamales, M., McGovern, A.E.*, et al.* Local D2- to D1-neuron transmodulation
1025 updates goal-directed learning in the striatum. *Science* **367**, 549-555 (2020).
1026 99. Kwak, S. & Jung, M.W. Distinct roles of striatal direct and indirect pathways in
1027 value-based decision making. *eLife* **8**, e46050 (2019).
1028 100. O'Hare, J.K., Ade, K.K.*, et al.* Pathway-Specific Striatal Substrates for Habitual
1029 Behavior. *Neuron* **89**, 472-479 (2016).
1030 101. Renteria, R., Cazares, C.*, et al.* Mechanism for differential recruitment of
1031 orbitostriatal transmission during actions and outcomes following chronic alcohol
1032 exposure. *eLife* **10** (2021).
1033 102. Stalnaker, T.A., Berg, B., Aujla, N. & Schoenbaum, G. Cholinergic Interneurons
1034 Use Orbitofrontal Input to Track Beliefs about Current State. *J Neurosci* **36**, 6242-6257
1035 (2016).

1036 103. Hirokawa, J., Vaughan, A., Masset, P., Ott, T. & Kepecs, A. Frontal cortex neuron
1037 types categorically encode single decision variables. *Nature* **576**, 446-451 (2019).
1038 104. Schoenbaum, G. & Shaham, Y. The role of orbitofrontal cortex in drug addiction:
1039 a review of preclinical studies. *Biol Psychiatry* **63**, 256-262 (2008).
1040 105. Groman, S.M., Keistler, C.*, et al.* Orbitofrontal Circuits Control Multiple
1041 Reinforcement-Learning Processes. *Neuron* **103**, 734-746 e733 (2019).
1042 106. Stalnaker, T.A., Liu, T.L., Takahashi, Y.K. & Schoenbaum, G. Orbitofrontal
1043 neurons signal reward predictions, not reward prediction errors. *Neurobiol Learn Mem*
1044 **153**, 137-143 (2018).
1045 107. Morris, R.W., Dezfouli, A., Griffiths, K.R., Le Pelley, M.E. & Balleine, B.W. The
1046 neural bases of action-outcome learning in humans. *J Neurosci* **42**, JN-RM-1079-1021
1047 (2022).
1048 108. Alexander, W.H. & Brown, J.W. Medial prefrontal cortex as an action-outcome
1049 predictor. *Nat Neurosci* **14**, 1338-1344 (2011).
1050 109. Rushworth, M.F. & Behrens, T.E. Choice, uncertainty and value in prefrontal and
1051 cingulate cortex. *Nat Neurosci* **11**, 389-397 (2008).
1052 110. Hart, G., Bradfield, L.A. & Balleine, B.W. Prefrontal Corticostriatal Disconnection
1053 Blocks the Acquisition of Goal-Directed Action. *J Neurosci* **38**, 1311-1322 (2018).
1054 111. Koob, G.F. Alcoholism: Allostasis and Beyond. *Alcohol Clin Exp Res* **27**, 232-243
1055 (2003).
1056 112. Jayaram-Lindström, N., Ericson, M., Steensland, P. & Jerlhag, E. Dopamine and
1057 Alcohol Dependence: From Bench to Clinic. in *Recent Advances in Drug Addiction*
1058 *Research and Clinical Applications* (2016).

1059 113. Groman, S.M., Rich, K.M., Smith, N.J., Lee, D. & Taylor, J.R. Chronic exposure to
1060 methamphetamine disrupts reinforcement-based decision making in rats.
1061 *Neuropsychopharmacology : official publication of the American College of*
1062 *Neuropsychopharmacology* **43**, 770-780 (2018).
1063 114. Brown, V.M., Zhu, L.*, et al.* Reinforcement Learning Disruptions in Individuals With
1064 Depression and Sensitivity to Symptom Change Following Cognitive Behavioral Therapy.
1065 *JAMA Psychiatry* **78**, 1113-1122 (2021).
1066 115. Wiehler, A., Chakroun, K. & Peters, J. Attenuated Directed Exploration during
1067 Reinforcement Learning in Gambling Disorder. *J Neurosci* **41**, 2512-2522 (2021).
1068 116. Kalhan, S., Schwartenbeck, P., Hester, R. & Garrido, M.I. People with a tobacco
1069 use disorder exhibit misaligned Bayesian belief updating by falsely attributing non-drug
1070 cues as worse predictors of positive outcomes compared to drug cues. *Drug and Alcohol*
1071 *Dependence* **256**, 111109 (2024).
1072 117. Vendruscolo, L.F. & Roberts, A.J. Operant alcohol self-administration in
1073 dependent rats: focus on the vapor model. *Alcohol* **48**, 277-286 (2014).
1074 118. Gilpin, N.W., Richardson, H.N., Cole, M. & Koob, G.F. Vapor inhalation of alcohol
1075 in rats. *Curr Protoc Neurosci* **9**, 29 (2008).
1076 119. Ottenheimer, D.J., Wang, K.*, et al.* Reward activity in ventral pallidum tracks
1077 satiety-sensitive preference and drives choice behavior. *Science Advances* **6**, eabc9321
1078 (2020).
1079 120. Ottenheimer, D.J., Bari, B.A.*, et al.* A quantitative reward prediction error signal in
1080 the ventral pallidum. *Nat Neurosci* (2020).

121. Ottenheimer, D., Richard, J.M. & Janak, P.H. Ventral pallidum encodes relative reward value earlier and more robustly than nucleus accumbens. *Nat Commun* **9**, 4350 (2018).

122. Meehan, C., Ebrahimian, J., Moore, W. & Meehan, S. Uniform Manifold Approximation and Projection (UMAP). (MATLAB Central File Exchange, https://www.mathworks.com/matlabcentral/fileexchange/71902, 2022).

123. Carpenter, B., Gelman, A.*, et al.* Stan: A probabilistic programming language. *Journal of statistical software* **76** (2017).

124. Bowling, S.R., Khasawneh, M.T., Kaewkuekool, S. & Cho, B.R. A logistic approximation to the cumulative normal distribution. *Journal of industrial engineering and management* **2**, 114-127 (2009).

125. Vehtari, A., Gelman, A. & Gabry, J. Practical Bayesian model evaluation using leave-one-out cross-validation and WAIC. *Statistics and Computing* **27**, 1413-1432 (2017).

126. Elber-Dorozko, L. & Loewenstein, Y. Striatal action-value neurons reconsidered. *Elife* **7** (2018).

Figures and Figure legends

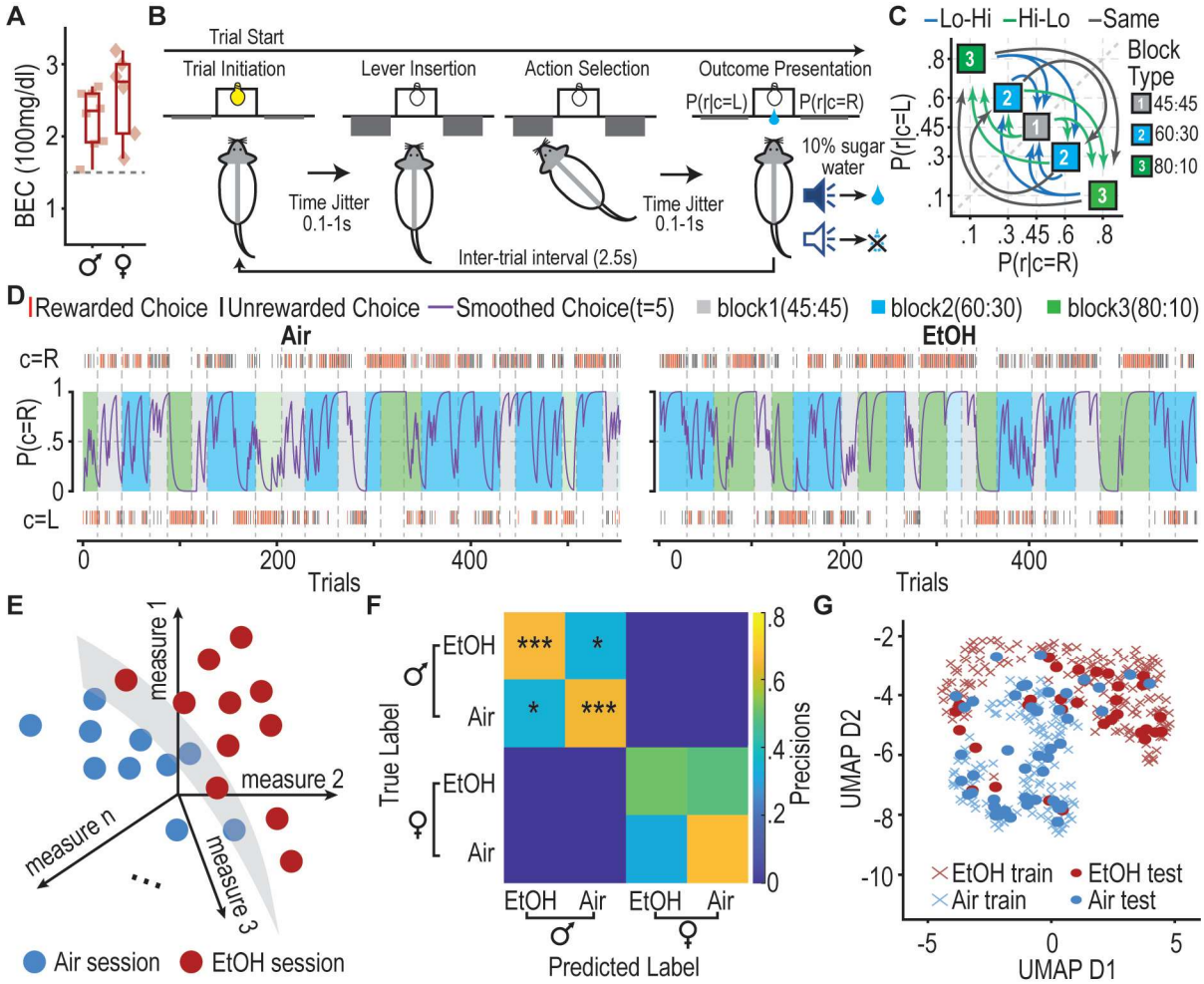

Figure 1. Ethanol-exposed rats exhibit a distinct pattern of behavior in the dynamic probabilistic reversal learning task (dynaPRL) after prolonged withdrawal. (**A**) Blood ethanol (EtOH) concentrations (BEC) of male and female rats during EtOH vapor exposure. t(12) = -1.24, p = 0.239, t test. (**B**) Schematic of trial structure showing each behavioral stage in the dynaPRL task. Trials began with a magazine entry (trial initiation). After a random time interval between 100ms to 1s (time jitter), both levers were inserted. After the rat pressed one of the levers, the levers were withdrawn. Following another time jitter, an outcome was reported. A rewarded choice was indicated by a clicker sound, followed by sucrose, and an unrewarded choice was indicated by white noise. P(r|c=L)

1109 represents the reward (r) probability given choice (c) is left side (L). (**C**) Choice reward
1110 probabilities for the dynaPRL task. The reward probabilities associated with each lever
1111 switched between 3 distinct blocks, drawing probabilities from three different sets, (0.8,
1112 0.1), (0.6,0.3), and (0.45, 0.45). Based on the difference of reward probabilities between
1113 two levers before and after block transition, all block transitions can be categorized into
1114 three types: low to high (LH) challenge, high to low (HL) challenge, and same to same
1115 (no difference, ND) are denoted as lines with distinct colors. (**D**) Two example rats from
1116 air (left) and EtOH (right) groups exhibit choice behavior that changes according to block
1117 switching. Choice raster, whether rewarded or not, are depicted with distinct colors. The
1118 letter 'c' denotes the side of choice, with 'L' for left and 'R' for right. The probability of
1119 choosing the right side, denoted as P(c=R), is calculated using a moving average across
1120 a window of 5 trials, thus providing a smoothed estimate of choice behavior (t=5). (**E**) This
1121 schematic illustrates how a support vector, depicted by the grey surface, differentiates
1122 between sessions from EtOH-exposed rats and control (air-exposed) rats, represented
1123 as dots, within the multidimensional space created by various behavioral measurements.
1124 This illustration represents our hypothesis that ethanol (EtOH)-exposed and air-exposed
1125 groups likely establish distinct behavioral patterns. (**F**) Confusion matrix for the SVM
1126 multiclass classifier aggregating from 1000 iterations in decoding both group and sex for
1127 n = 13 EtOH rats (8 male, 5 female) and 14 air controls (9 male, 5 female). Entries on the
1128 primary diagonal represent accurate predictions, and off-diagonal elements represent
1129 misclassifications. Classification precision was calculated based on the true positive
1130 rate/(true positive rate + false positive rate). *$p < 0.05$, ***$p < 0.001$, Monte Carlo

1131 significance tests. (**G**) An UMAP transformation of high dimensional data onto a 2D

1132 space.

1133

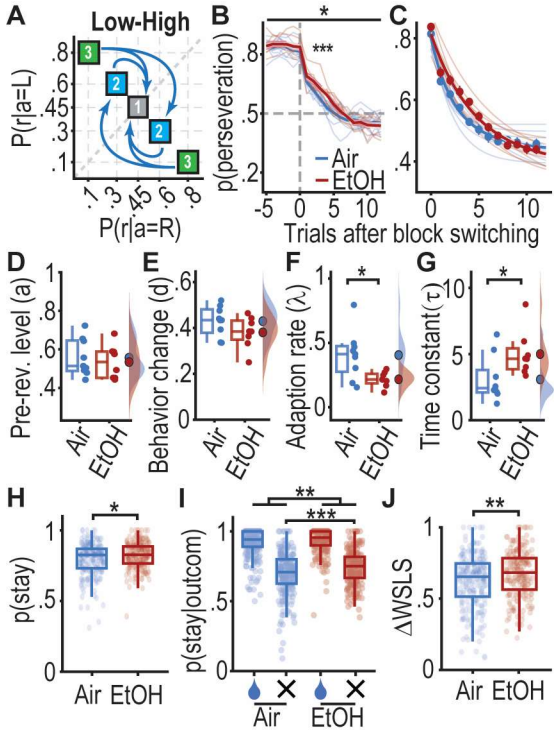

Figure 2. Protracted withdrawal from chronic ethanol exposure alters choice behaviors in highly ambiguous environments. (**A, B**) The diagram illustrates block switching in Low-High uncertainty transitions (A). Probability of choosing the pre-switch preferred lever in Low-High type transitions (B). Bolded lines represent the group average and faded lines represent individual rats. Vertical dashed line indicates the last trial before block switching (t=0). F(1, 16) = 1.708, p = 0.211 main effect of group; F(16,255) = 362.055, ***p = 1.2E-167, main effect of time; F(16,255) = 1.925, *p = 0.016, interaction of group and time, two-way mixed-effect ANOVA. *p < 0.05 for post hoc test, two-way mixed-effect ANOVA followed by post hoc test with Bonferroni correction. (**C**) A single exponential decay model estimated the performance in learning new action-outcome contingency. Bolded lines show the average model fit for probability of selecting an action based on the pre-switch contingencies. Dots depict the true mean data from B. Individual rat model estimates of choice probability are shown in faded lines. (D-G) The estimated parameters' pre-reversal asymptotic value (pre-rev. level), a (D); magnitude of change in

1148 p(preservation) (behavior change), d (E); and adaptation rate, λ (F) for the single
1149 exponential decay model in C. The inverse of λ, τ, represents the time constant of rat's
1150 learning in a new block (G). The box plot depicts the median, 25th, and 75th percentile of
1151 the parameter values for each group. Each dot next to the box plot shows parameter
1152 values from individual rats. The cloud plot on the right side of each panel depicts the data
1153 distribution. Dots on the cloud plot are the mean of the parameter values. t(15) = -0.498,
1154 p = 0.626 for D; t(15) = -1.522, p = 0.149 for E; t(15) = -2.704, *p = 0.016 for F; t(15) =
1155 2.300, *p = 0.036 for G, two-sample independent t test with two-tails. n = 9,8 rats for Air
1156 and CIE groups for B-G. (**H**) Stay probability, the likelihood of rats repeating the same
1157 action on the current trial as the last trial, during 'Lo-Hi' transitions. z(464) = -2.358, *p =
1158 0.018, Wilcoxon rank-sum test. (**I**) Stay probability given reward (water drop icon) or no
1159 reward (cross, X, symbol) on the last trial, during 'Lo-Hi' transitions. F(1, 463) = 1076.3,
1160 ***p = 7.3E-123 main effect of outcomes; F(1, 463) = 10.625, **p = 0.001 main effect of
1161 group; and F(1, 463) = 4.5, *p = 0.035 for interaction of outcome and group, two-way
1162 mixed-effect ANOVA. ***p < 0.001 for post hoc test with Bonferroni correction. (**J**)
1163 Difference (Δ) between probability of stay given reward (win-stay, WS) and probability of
1164 shift given no reward (lose-shift, LS), ΔWSLS, during 'Lo-Hi' transitions. z(464) = -2.805,
1165 **p = 0.005, Wilcoxon rank-sum test. N = 241, 229 sessions from 9, 8 male rats for air
1166 and EtOH for A-J.

1167

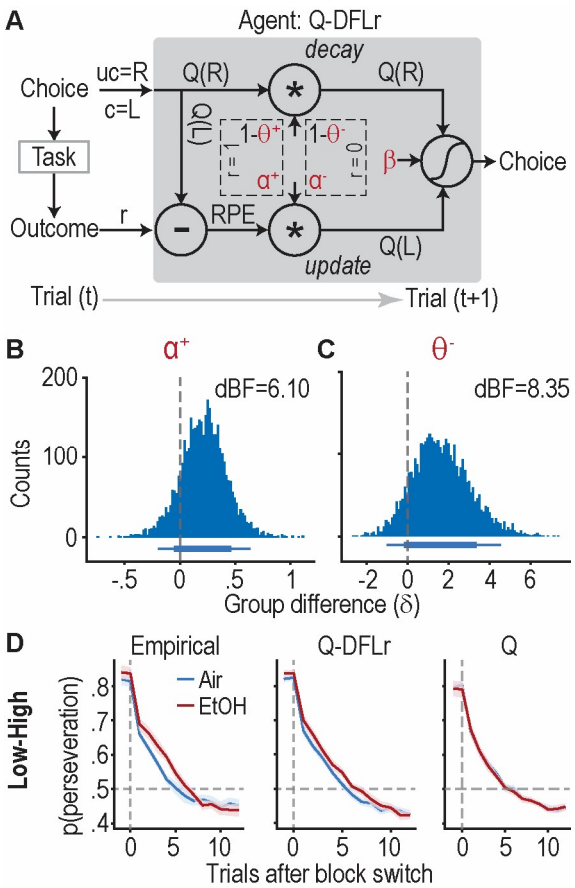

Figure 3. EtOH enhances positive feedback-mediated learning rates and negative feedback-mediated forgetting rates in the reinforcement learning process. (**A**) Schematic representation of the value updating processes employed by the best-fitting reinforcement learning (RL) agent, Q-DFLr. In this example, an agent makes a left side choice at trial, t, denoted as 'c=L', where ‘c’ stands for ‘choice’. In contrast, 'uc=R' indicates the right lever was not selected, where ‘uc’ stands for ‘unchosen’, meaning the right option was not selected. Upon making choice on left side, the task generates an outcome, 'r', where '1' signifies a reward, i.e., positive feedback, and '0' signifies absence of a reward, i.e., negative feedback. The left action value, Q(L)—or the chosen value—is updated based on the reward prediction error (RPE) using two distinct learning rates, α^+ for reward (r=1) and α^- for non-reward (r=0) action outcomes. Conversely, the right action

value, Q(R)—or the unchosen value—undergoes decay at two distinct forgetting rates, θ^+ and θ^-, depending on the action outcome, r. The updated action values are then adjusted by the inverse temperature parameter, β, to inform the agent's next choice (t+1) via a softmax selection function. (**B**,**C**) HMC-sampled posterior densities of group difference, δ, representing differences between EtOH- and air-exposed rats in positive feedback-mediated learning rates (α^+) in (B) and negative feedback-mediated forgetting rates (θ^-) in (C), across group-level hyperparameters. Bottom horizontal lines represent the 80% and 95% highest density interval (HDI). dBF: directed Bayes factor. (**D**) Choice probability of the initially preferred lever in low-to-high transitions. Data on the left panel are empirical (reproduced from Figure 1G), while the right panel showcases simulated data using the best-fitting parameters.

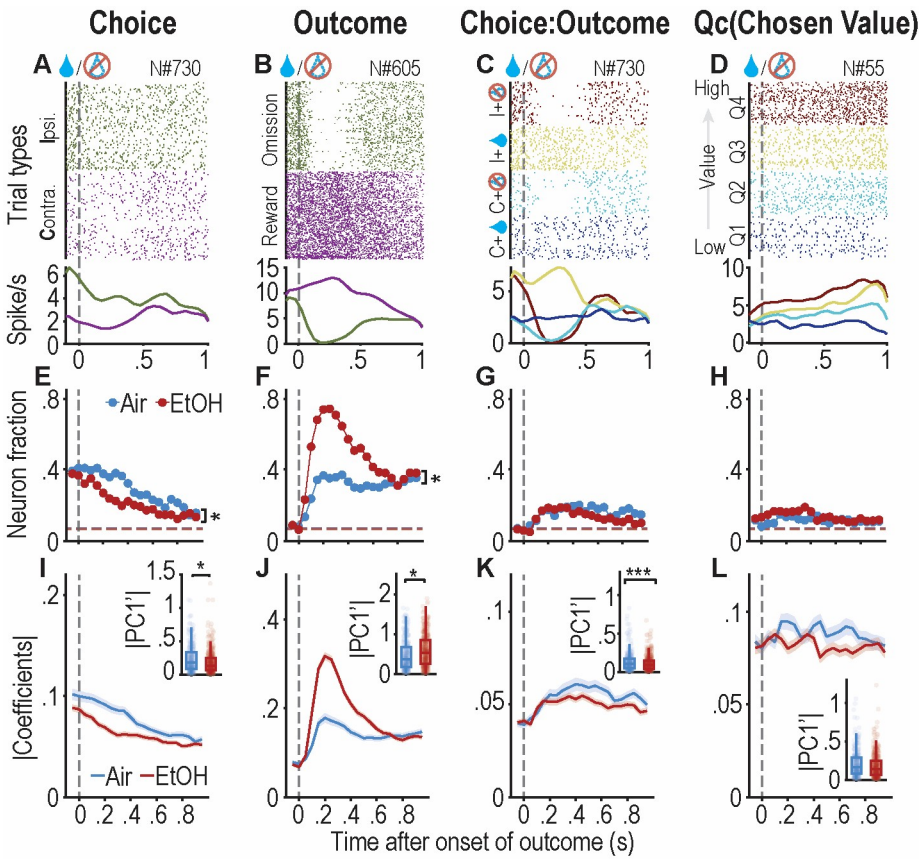

Figure 4. **EtOH alters the encoding of decision variables in the outcome presentation.** (**A-D**) An example DMS unit from the air group shows spike activity correlated with choice side (A), outcome (B), interaction of choice and outcome (labeled choice:outcome) (C), and the value of the chosen action, Qc (D). Trials were grouped by choice side as either ipsilateral (I) or contralateral (C) to the recording site in A; by outcome as rewarded (reward) or unrewarded in B; by contingency as ipsilateral choice without reward ('I' and no water drop icon), ipsilateral choice with reward ('I' and water drop icon), contralateral choice without reward ('C' and no water drop icon), and contralateral choice with reward ('C' and water drop icon) in C; and into quartiles of the chosen action value: Q1 (0-0.25), Q2 (0.25-0.5), Q3 (0.5-0.75), and Q4 (0.75-1) in D. At the top are spike raster plots. At the bottom are spike density functions generated by applying a Gaussian kernel (δ = 100 ms) to the corresponding spike trains from A-D. (**E-**

1203 **H**) Fraction of neurons whose activity is significantly modulated by the current trial's
1204 choice (E), outcome (F), choice:outcome interaction (G), and Qc (H). *p = 0.021 main
1205 effect of group for E, logistic regression with Generalized Linear Mixed-Effect Model
1206 (GLMM); *p = 0.018 main effect of group for F, logistic regression GLMM; p = 0.47 main
1207 effect of group for H, logistic regression GLMM; p = 0.63 main effect of group for H, logistic
1208 regression GLMM. (**I-L**) The magnitude of the regression coefficient (|Coefficients|) for
1209 choice (I), outcome (J), choice:outcome interaction (K), and Qc (L) averaged across all
1210 neurons with the corresponding PC1 scores (|PC1'|) in the inset figures. ***p = 0.049 main
1211 effect of group for the inset figure in I, GLMM. *p = 0.041 main effect of group for the inset
1212 figure in J, GLMM. ***p = 0.0004 main effect of group for the inset figure in K, GLMM. p =
1213 0.47 main effect of group for the inset figure in L, GLMM. n = 326, 523 neurons from 9,8
1214 male rats in air and EtOH groups.

1215

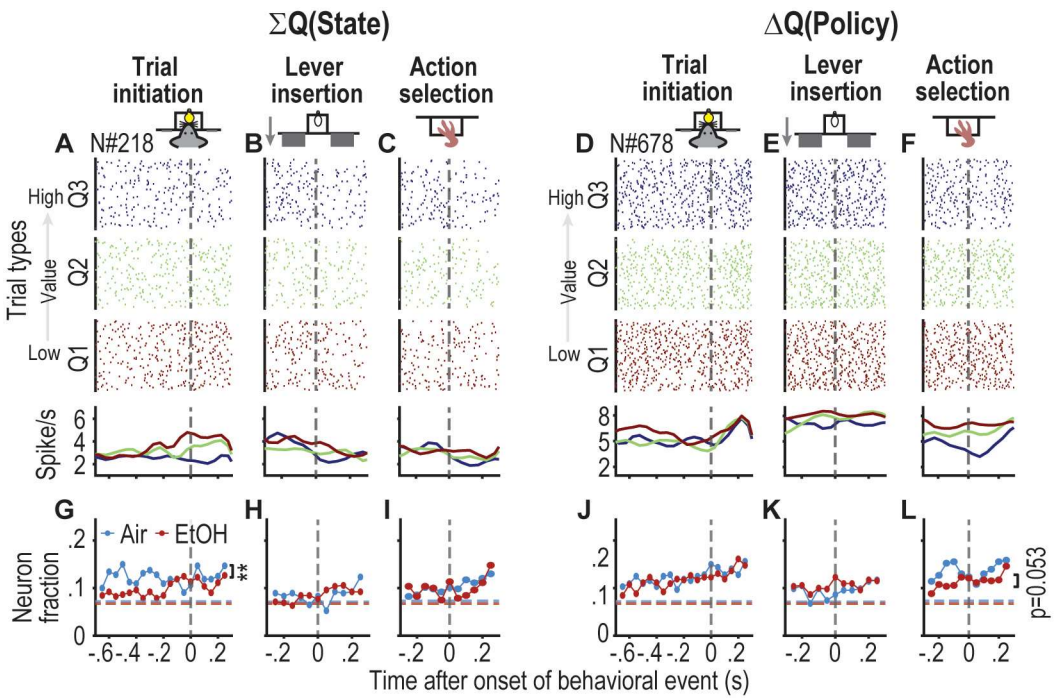

Figure 5. CIE alters the encoding of decision variables in the action selection epoch. (**A-C**) An example DMS unit from the air group shows spike activity correlated with value of state, ΣQ, around trial initiation (A), lever insertion (B), and action selection (C). Trials were grouped by three quartiles of the state value: Q1 (0-0.33), Q3 (0.34-0.66), and Q3 (0.67-1) in A-C. At the top are spike raster plots. At the bottom are spike density functions generated by applying a Gaussian kernel (δ = 100 ms) to the corresponding spike trains from A-D. (**D-F**) An example DMS unit from the air group shows spike activity correlated with policy values, ΔQ, around trial initiation (D), lever insertion (E), and lever press (F). Trials were grouped by three quartiles of the policy value from low to high (bottom to top). Spike density functions at the bottom panels are estimated same as A-C. (**G-I**) Fraction of neurons whose activity is significantly modulated by the state value, ΣQ, in the period of trial initiation (G), lever insertion (H), and lever press (I). **p = 0.004 main effect of group for G, logistic regression with Generalized Linear Mixed-Effect Model (GLMM). (**J-L**) Fraction of neurons whose activity is significantly modulated by the state value, ΔQ, in

1230 the period of trial initiation (J), lever insertion (K), and lever press (L). $p = 0.053$ main
1231 effect of group for L, GLMM. figures. $n = 326, 523$ neurons from 9,8 male rats in air and
1232 EtOH groups.

1233

1234 **Figure S1**

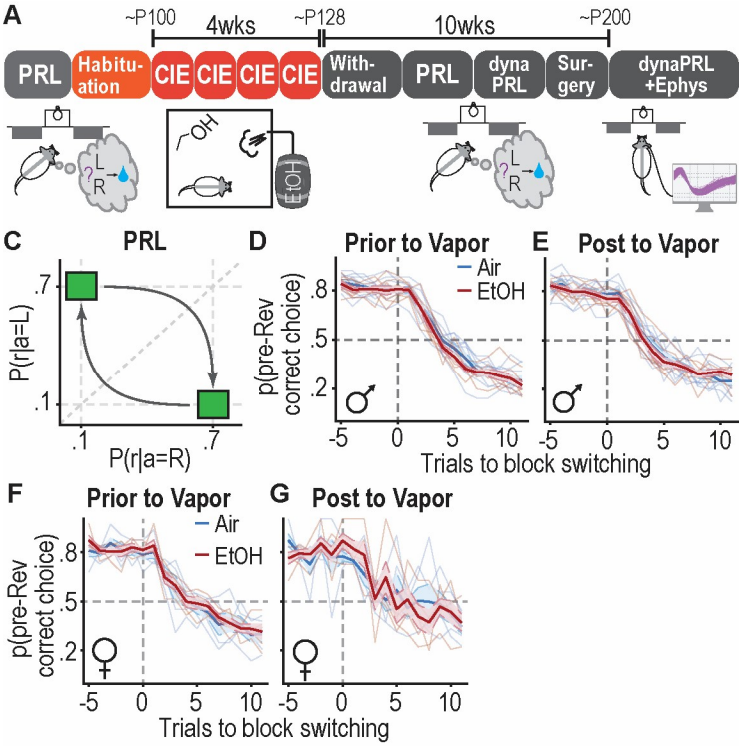

1235 **Figure S1. Protracted withdrawal from chronic ethanol exposure does not impair**
1236 **reversal learning in traditional probabilistic reversal learning task.** (**A**) Experimental
1237 timeline: Rats underwent training in a simple probabilistic reversal learning (PRL) task to
1238 counterbalance their behaviors prior to 4-week chronic ethanol vapor exposure (CIE)
1239 procedure with a preceding habituation phase for acclimatization to ethanol vapor and
1240 experimental environment. Following 10-15 days of withdrawal, rats were retrained with
1241 the PRL task and then introduced to a new task, the dynamic probabilistic reversal
1242 learning (dynaPRL) task. 16-channel drivable electrodes were implanted in rats. After
1243 recovery and retraining, single-unit activity was recorded. (**B**) Choice reward probabilities
1244 for the PRL task. The reward probabilities associated with each lever switched within one
1245 block type drawing probability from a set (0.7, 0.1). (**C,D**) Probability of choosing pre-
1246 reversal preferred lever before (C) and after (D) CIE vapor in males. N = 9,8 male rats for
1247 Air and CIE groups. (**E**,**F**) Probability of choosing pre-reversal preferred lever before (E)

1248 and after (F) CIE vapor in females. N = 5,5 female rats for Air and CIE groups. Bolded
1249 lines represent the group average and faded lines represent individual rats. Vertical
1250 dashed line indicates the last trial before block switching (t=0) for D-G.

1251

1252 **Figure S2**

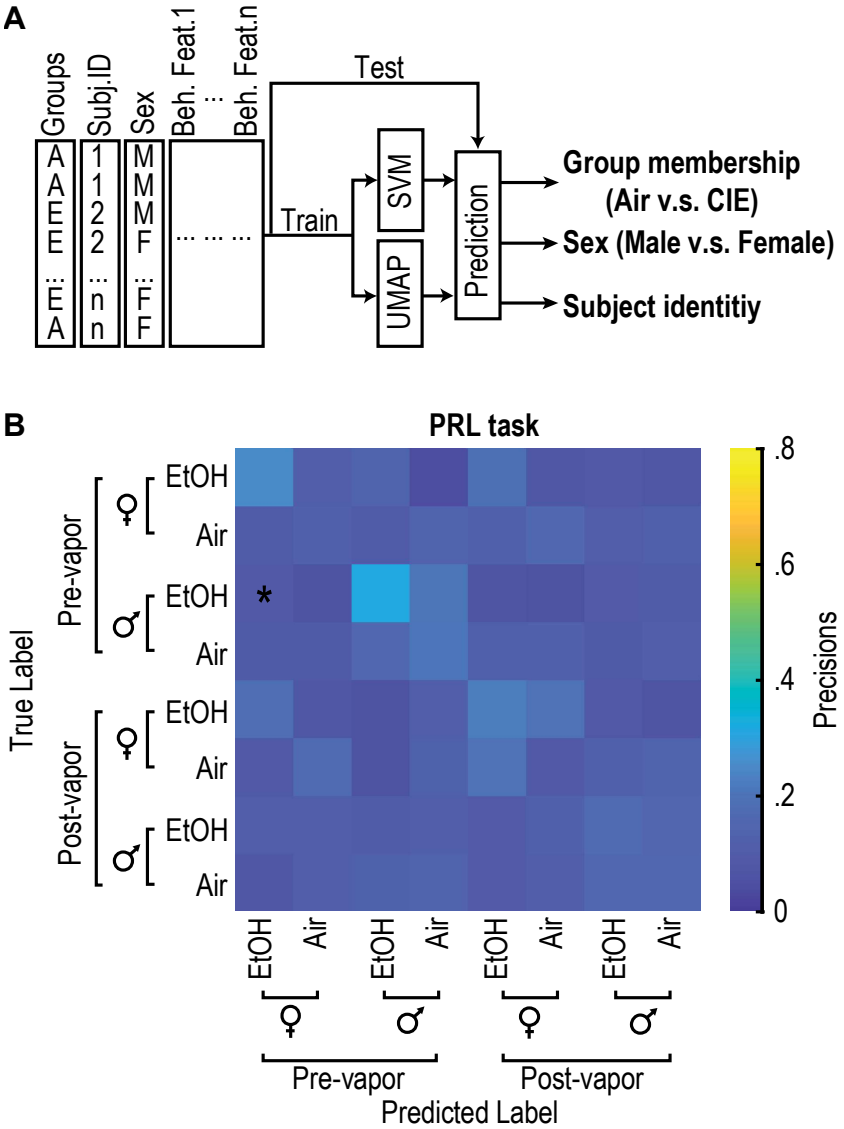

1253 **Figure S2. EtOH-exposed rats do not exhibit a distinct behavioral pattern in the PRL**
1254 **task.** (**A**) The diagram illustrates the classification analysis process. (**B**) Confusion matrix
1255 for the SVM multiclass classifier aggregating from 1000 iterations in decoding group
1256 membership (EtOH vs. Air), sex label, and exposure conditions (pre- v.s. post-vapor) for
1257 N = 13 EtOH rats (8 male, 5 female) and 14 air controls (9 male, 5 female). Diagonal
1258 entries represent accurate predictions, while off-diagonal elements represent
1259 misclassifications. Classification precision is computed from true positive rate/(true

1260 positive rate + false positive rate). *$p < 0.05$ indicates statistical significance determined

1261 through Monte Carlo significance tests.

1262

Figure S3

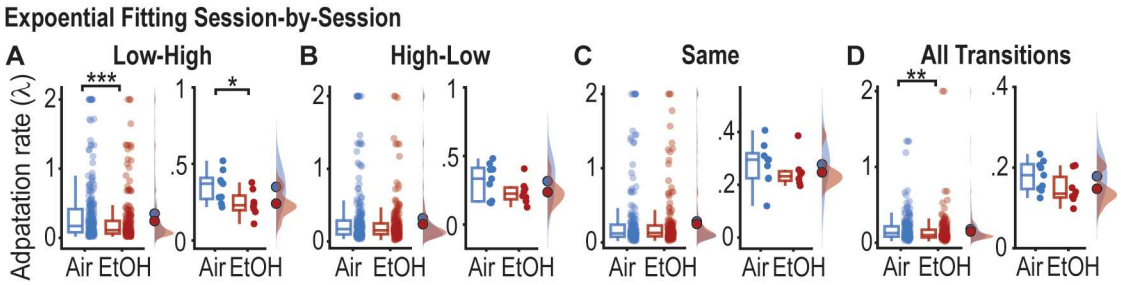

Figure S3. The adaptation rate (λ) is estimated across individual sessions in the dynaPRL task. (**A-D**) The adaptation rates (λ) in Low-High (A), High-Low (B), and Same (C) type transitions, as well as trials of all types of transitions (D) from individual sessions, are presented in the left panel in A-D. **p < 0.01, ***p < 0.001, Wilcoxon rank-sum test. The adaptation rates (λ) for each rat, averaged from individual sessions, are shown in the right panel of A-D. *p < 0.05, two-sample independent t test with two-tails. In the left panels, dots represent individual sessions. In the right panels, dots represent individual rats. The box plot depicts the median, 25th, and 75th percentile of the parameter values for each group. N = 241 sessions from 9 male air rats and 229 sessions from 8 male EtOH rats.

Figure S4

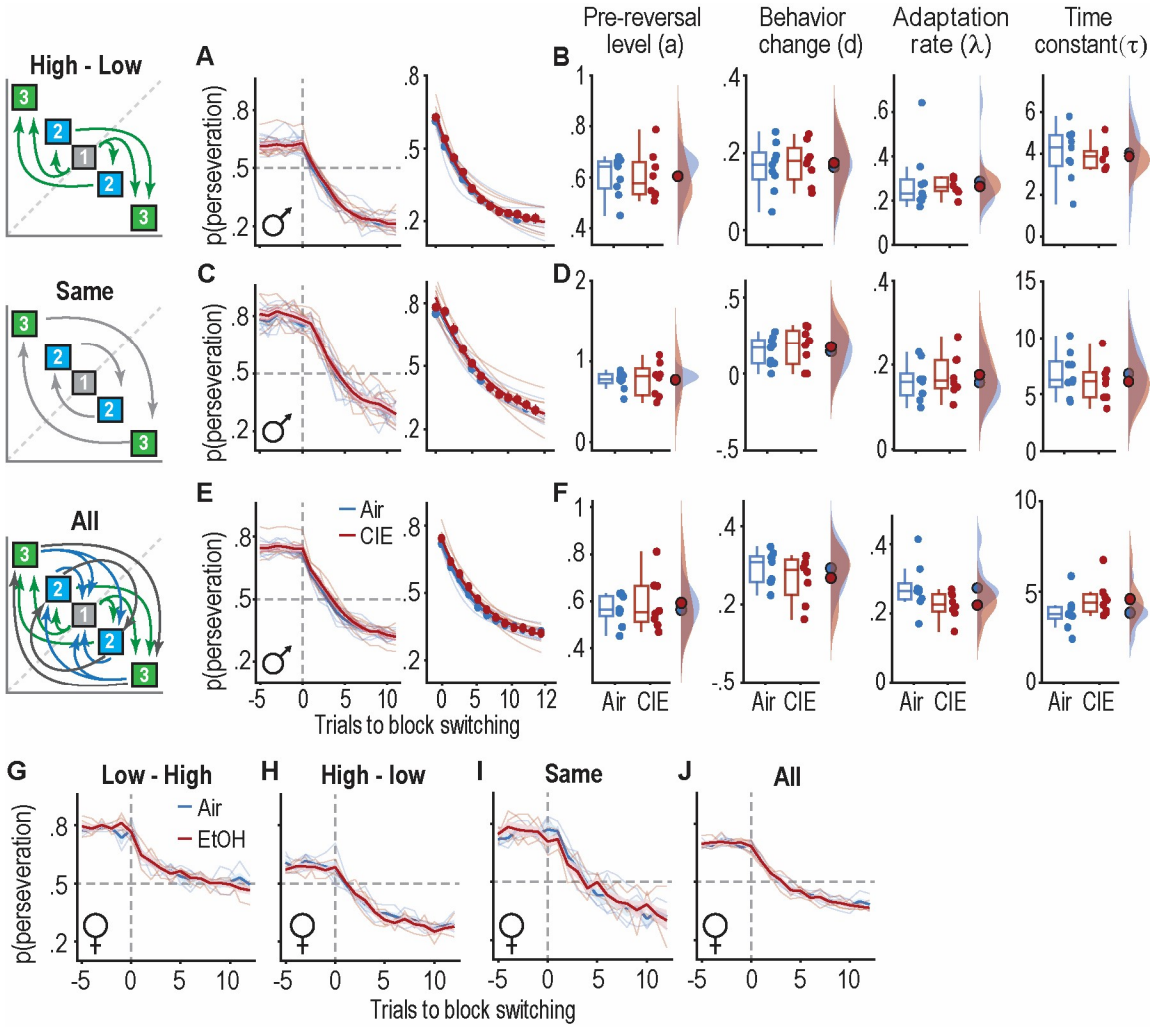

Figure S4. Pre-EtOH exposure does not alter reversal learning under low uncertainty in the dynaPRL task. (**A-F**) The probability of selecting the preferred lever before the block switching (left panel) and the performance estimated by the single exponential decay model for learning new action-outcome contingency (right panel) during transitions with High-Low (A), Same (C), and transitions aggregate from all types (E) in male rats. In the left panels, bold lines indicate the average model fit for the probability of selecting an action based on the pre-switch contingencies. In the right panels, dots represent the true mean data from A, C, and E, and faded lines illustrate model estimates of individual rat choice probability. The estimated parameters' pre-

reversal asymptotic value (pre-rev. level), a; magnitude of change in p(preservation) (behavior change), d, adaptation rate, λ, and time constant, τ, for the single exponential decay model during transitions with High-Low (B), Same (D), and transitions aggregate from all types (F) in males. Dots represent individual rats. The box plot depicts the median, 25th, and 75th percentile of the parameter values for each group. (**G-J**) Probability of selecting pre-switching preferred lever in transitions with Low-High (G), High-Low (H), and Same (I) type transitions as well as transitions aggregate from all types (J) in females. Bold lines indicate the average model fit for the probability of selecting an action based on the pre-switch contingencies. N = 13 EtOH rats (8 male, 5 female) and 14 air controls (9 male, 5 female).

Figure S5

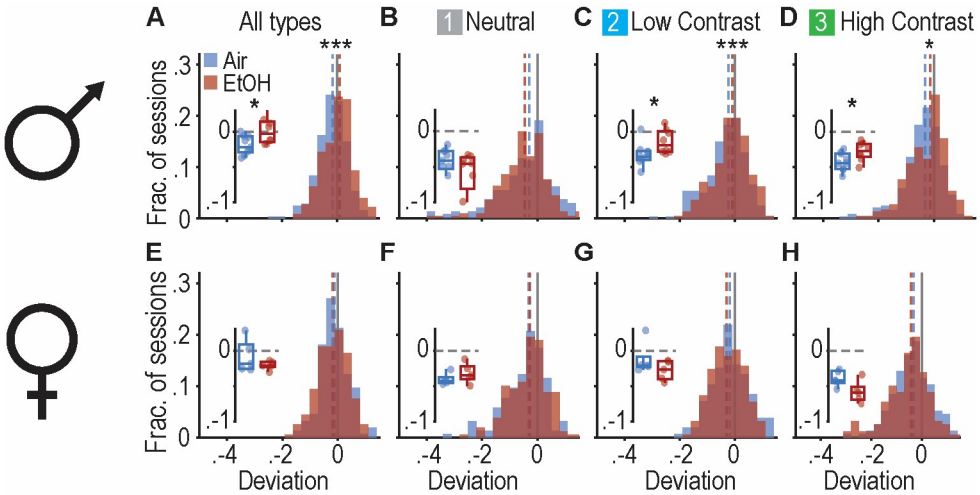

Figure S5. Pre-EtOH exposure reduces deviation from matching choice behavior to local reward rate in males but not in females. (**A-D**) Histograms reveal higher matching scores (deviation of choice probability from the reward probability given the choice) in trials from blocks aggregating from all types (A), and low contrast (C; 60,30), as well as high contrast (D; 80,10) blocks, but not from neutral blocks (B; 45, 45), in EtOH rats compared to air controls. Vertical blue and red dashed lines represent the median deviation from matching, while the vertical grey solid lines represent perfect matching (0 deviation of choice probability to reward probability given the choice). The inset panels demonstrate the mean deviation score averaged for each EtOH rat and air control, with each dot representing a rat. The horizontal dashed line marks the perfect matching. (**E-H**) Similar to A-D, histograms show no difference in matching scores in all (E), neutral (F), low contrast (G), and high contrast (H) type blocks. N = 13 EtOH rats (8 male, 5 female) and 14 air controls (9 male, 5 female).

1313 **Figure S6**

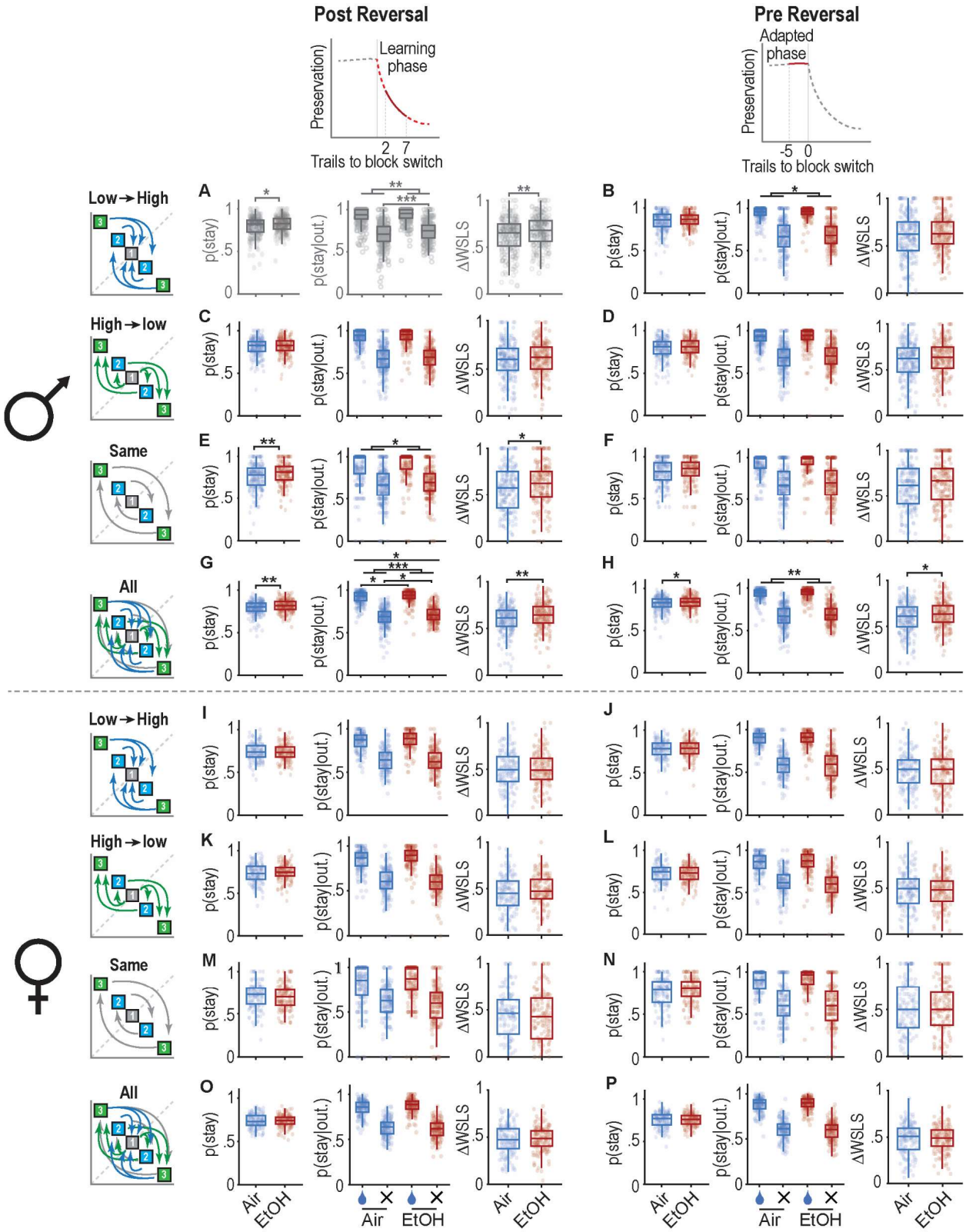

1314 **Figure S6. Stay probabilities in pre- and post-reversal under various cognitive**
1315 **challenges conditions.** (**A**-**H**) Stay probability (left panels), Stay probability given reward
1316 (water drop icon) or no reward (cross, X, symbol) on the last trial (middle panels), and
1317 difference of win-stay lose-switch probability (ΔWSLS; right panels) in the post-reversal
1318 (A, C, E, and G) and pre-reversal (B, D, F, and H) phases during various uncertainty
1319 conditions in males. Data in A is duplicated from Figures 2H-2J. (**I**-**P**) Stay probability (left
1320 panels), conditional stay probability (middle panels), and difference of win-stay lose-
1321 switch probability (ΔWSLS; right panels) in the pre-reversal (I, K, M, and O) and post-
1322 reversal (J, L, N, and P) phases during various uncertainty conditions in females. Dots
1323 represent individual sessions in air and EtOH groups. N = 241 sessions from 9 male air
1324 rats and 229 sessions from 8 male EtOH rats.

1325

1326

1327

1328

1329

1330 **Figure S7**

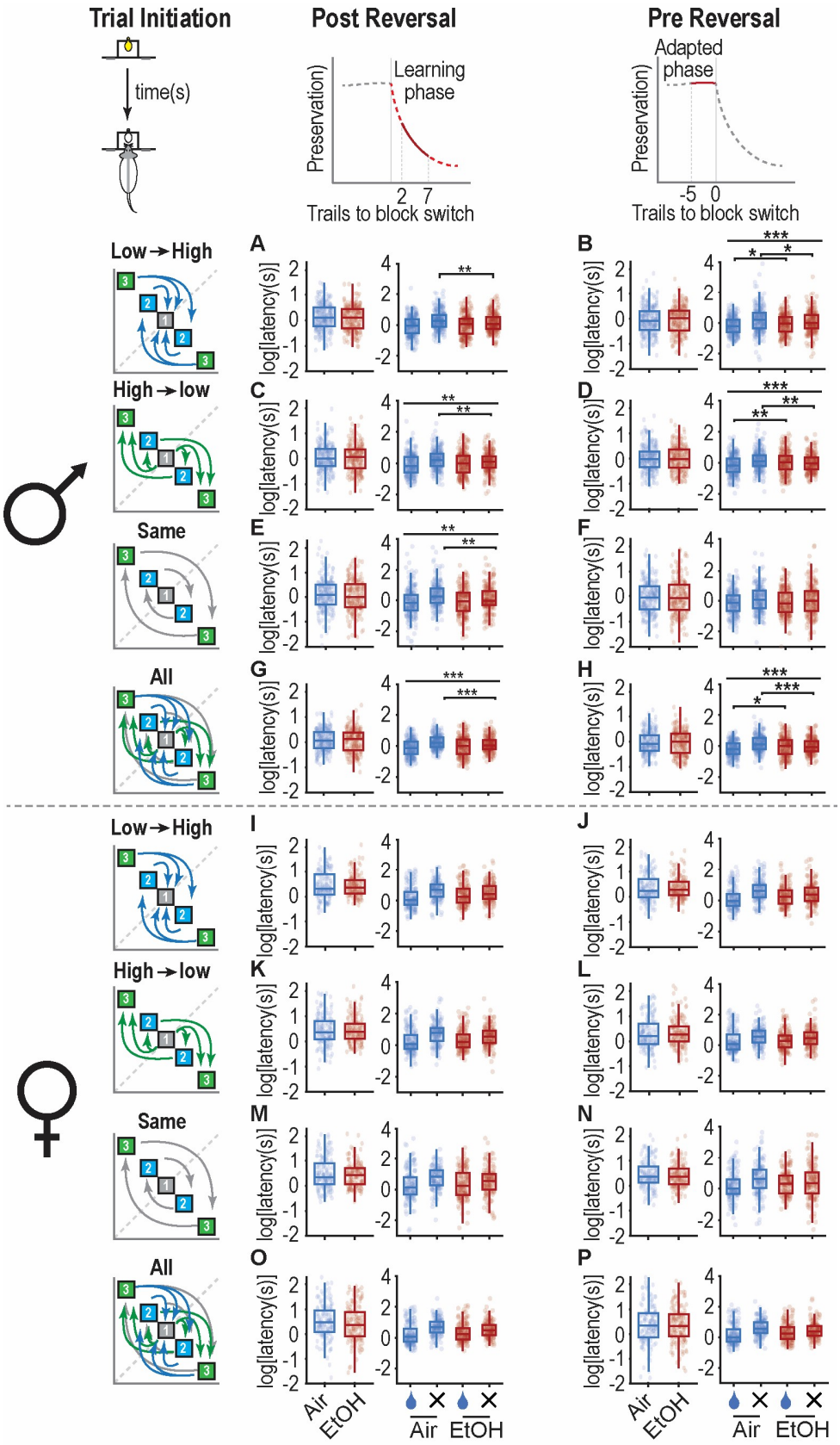

1331 **Figure S7. Latencies of trial initiation in pre- and post-reversal under various**
1332 **cognitive challenges conditions.** (**A**-**H**) General latency of trial initiation (left panels)
1333 and latency of trial initiation conditioned on last trial outcomes (right panels) in the post-
1334 reversal (A, C, E, and G) and pre-reversal phases (B, D, F, and H) under various
1335 transitions in males. (**I**-**P**) General latency of trial initiation (left panels) and latency of trial
1336 initiation conditioned on last trial outcomes (right panels) in the post-reversal (A, C, E,
1337 and G) and pre-reversal phases (B, D, F, and H) under various transitions in females.
1338 Dots represent individual sessions in air and EtOH groups. N = 241 sessions from 9 male
1339 air rats and 229 sessions from 8 male EtOH rats.

1340

1341

1342 **Figure S8**

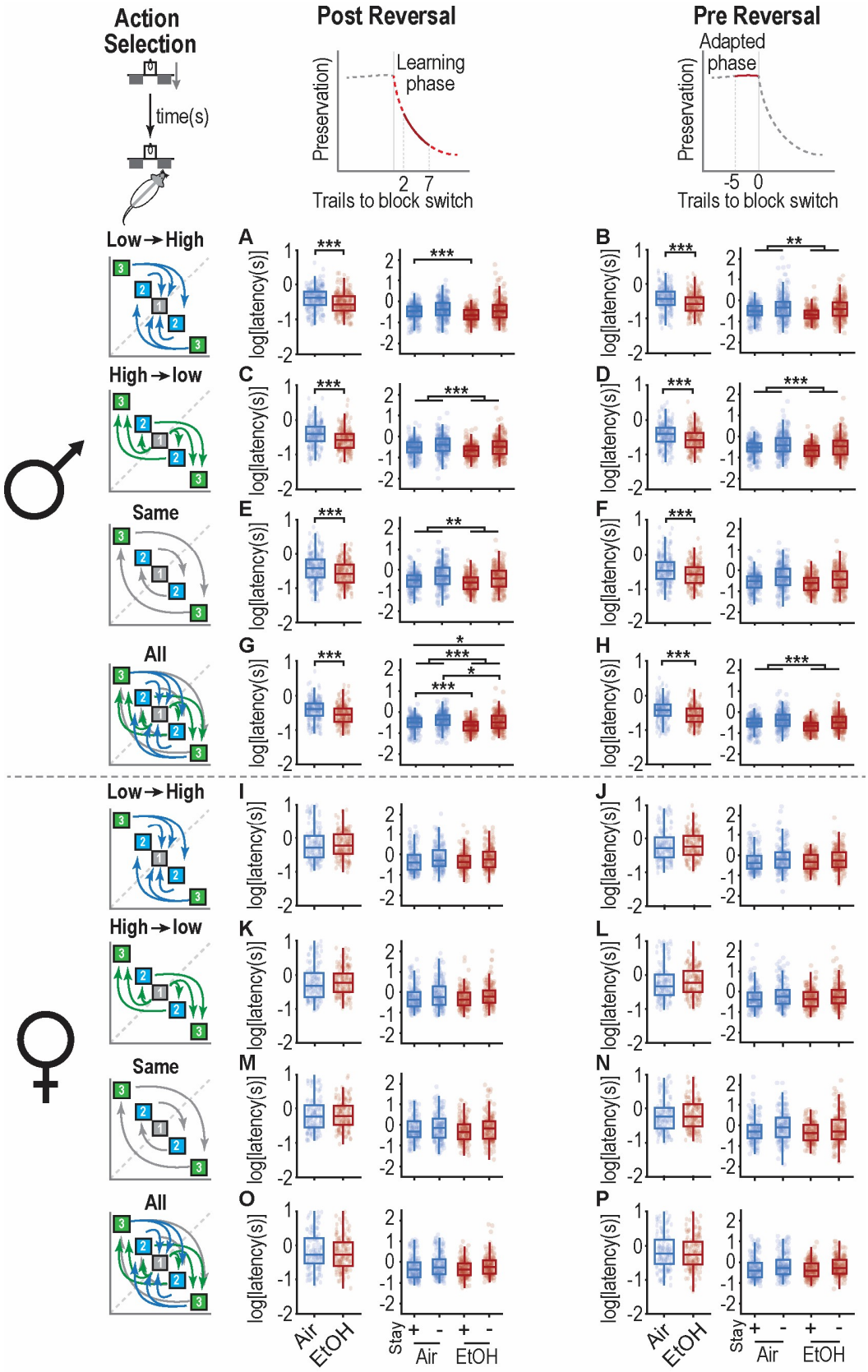

1343 **Figure S8. Latencies of action selection in pre- and post-reversal under various**
1344 **cognitive challenges conditions.** (**A**-**H**) General latency of action selection (left panels)
1345 and latency of trial initiation conditioned on last trial outcomes (right panels) in the post-
1346 reversal (A, C, E, and G) and pre-reversal phases (B, D, F, and H) under various
1347 transitions in males. (**I**-**P**) General latency of trial initiation (left) and latency of trial initiation
1348 conditioned on last trial outcomes (right) in the post-reversal (A, C, E, and G) and pre-
1349 reversal phases (B, D, F, and H) under various transitions in females. Dots represent
1350 individual sessions in air and EtOH groups. N = 241 sessions from 9 male air rats and
1351 229 sessions from 8 male EtOH rats.

1352

1353

Figure S9

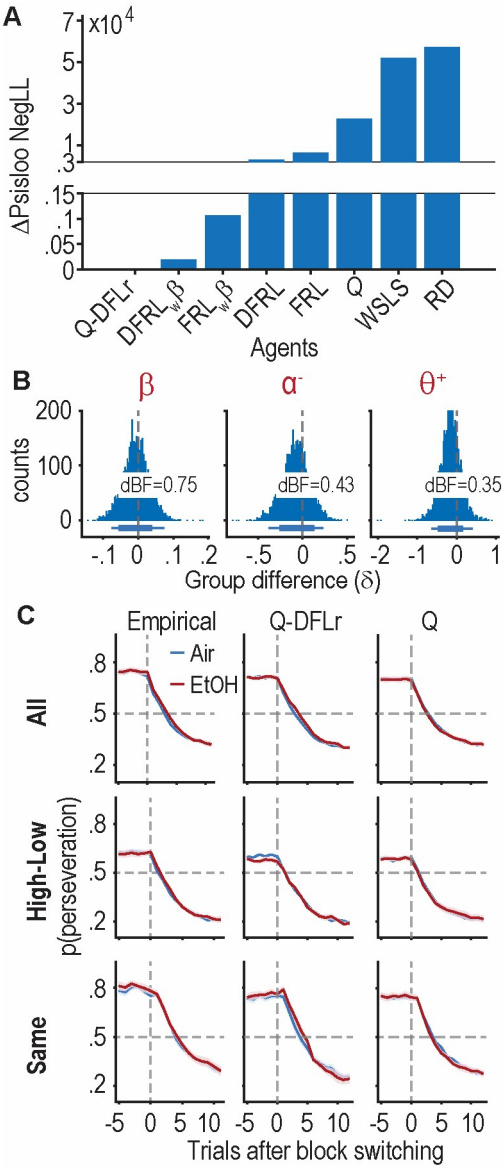

Figure S9. Reinforcement learning models fit trial-by-trial data from the dynaPRL task. (**A**) The bar plot showed the difference of Pareto-smoothed importance sampling (PSIS) with leave-one-out (LOO) negative likelihood (ΔPsisloo NegLL) between candidate models and the best fitting model, Q learning model with differential learning rate (Q-DFLr), on the most left on the x-axis. (**B**) HMC-sampled posterior densities of group difference, δ, representing differences between EtOH- and air-exposed rats in inverse temperature (β in the left panel), negative feedback-mediated learning rates (α^-

in the middle panel), and positive feedback-mediated forgetting rates (θ^+ in the right panel), across group-level hyperparameters. Bottom horizontal lines represent the 80% and 95% highest density interval (HDI). dBF: directed Bayes factor. (**C**) Choice probability of the initially preferred lever in all, High-low, and Same transitions. Data on the left panel are empirical (reproduced from Figure 1G), while the right panel showcases simulated data using the best-fitting parameters.

1368 **Figure S10**

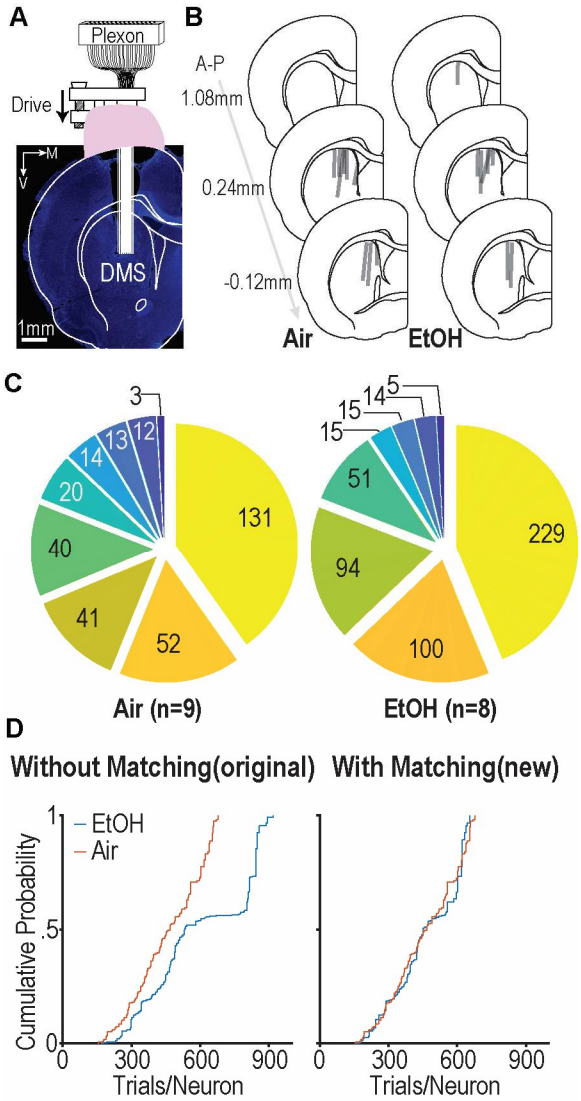

1369 **Figure S10. Single unit recording in the dorsomedial striatum (DMS).** (**A**) The
1370 diagram illustrates a drivable electrode consisting of 16 tungsten wires connected to a
1371 Plexon headstage, which is implanted in the Dorsomedial Striatum (DMS). (**B**) A
1372 visualization of electrode placement and the range of recording across sessions for each
1373 animal, denoted by grey lines. (**C**) Pie charts show the aggregate count of neurons
1374 recorded from each rat. (**D**) The cumulative probability distribution shows the number of
1375 trials for each recorded neuron before (left) and after (right) trial-matching, which is
1376 conducted between EtOH and air groups.

1377 **Figure S11**

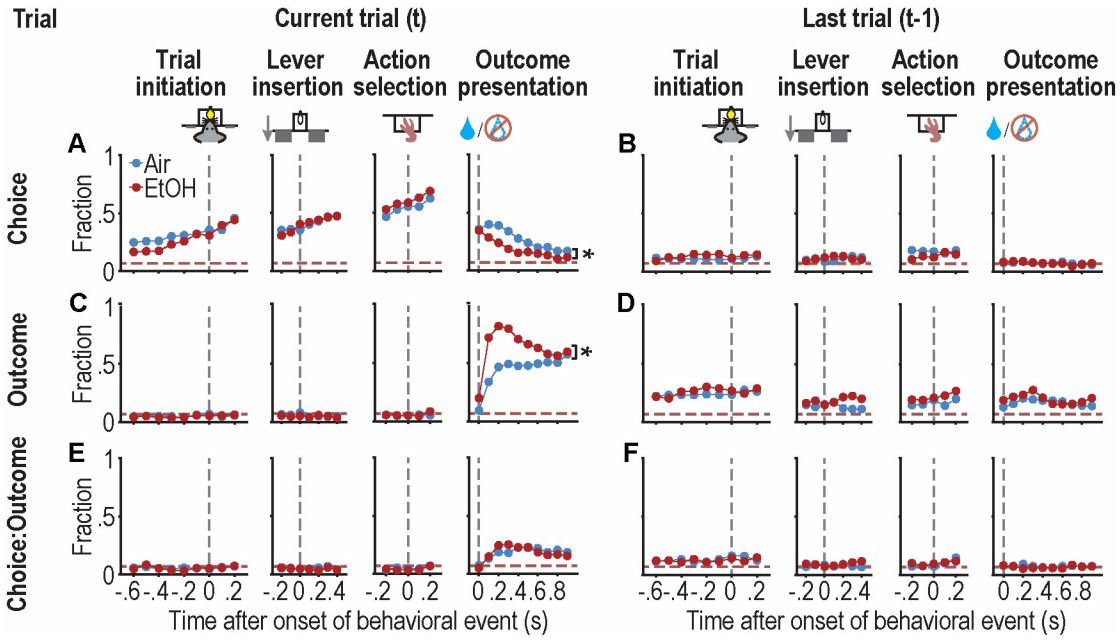

1378 **Figure S11. EtOH pre-exposure mainly alters the striatal choice and outcome**
1379 **signals in current trials.** (**A-F**) Fraction of neurons exhibiting significant modulation by
1380 choice (A and B), outcome (C and D), and the interaction of choice and outcome (E and
1381 F) in current trial and last trial around behavioral events such as trials initiation, lever
1382 insertion, lever press, and outcome report. Vertical grey dashed lines indicate the onset
1383 of each behavior event. Horizontal blue and red dashed lines indicate the chance level
1384 for air and EtOH groups, respectively. N = 326, 523 neurons from 9,8 male rats in air and
1385 EtOH groups.

1386

1387

1388 **Figure S12**

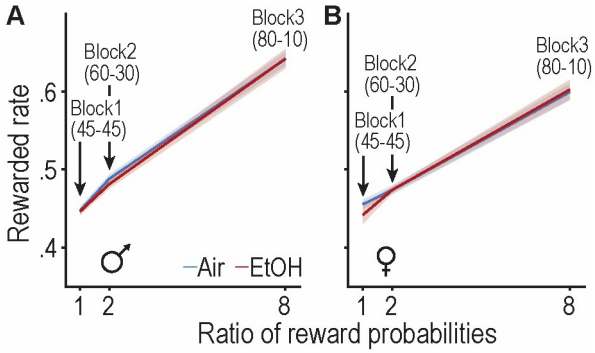

1389 **Figure S12. Reward rate as an indicator of block identity.** (**A**-**B**) Reward rates (ratio
1390 of rewarded trials to total trials) linearly increase in correlation with the reward probability
1391 ratios, ranging from block 1 (45:45) to block 3 (80:10) for both males (A) and females (B).
1392 N = 13 EtOH rats (8 males, 5 females) and 14 air controls (9 males, 5 females).

1393 **Figure S13**

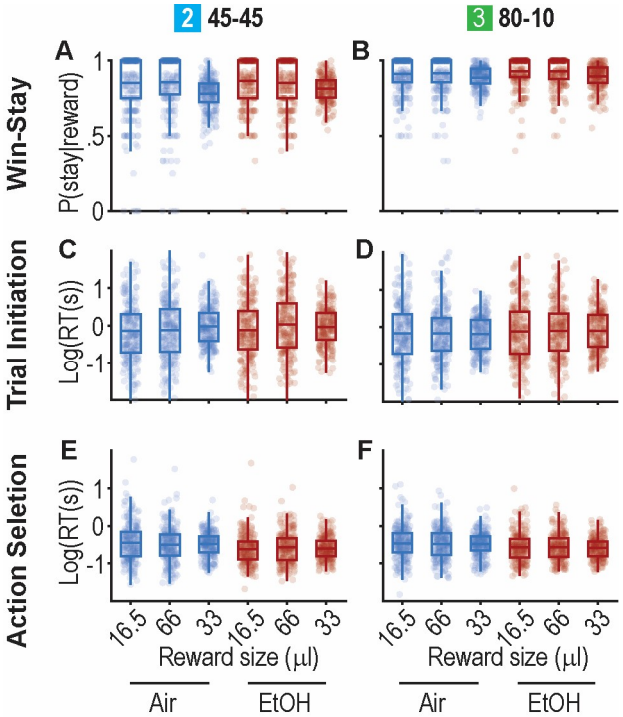

1394 **Figure S13. Rats do not respond to the size of the reward during the acquired phase**
1395 **in the dynaPRL task.** (**A-F**) The size of the reward is altered with a 40% chance by
1396 doubling or halving the reward size (66 μl or 16.5 μl) compared to the 60% original size
1397 (33 μl) 12-trial after switching to block2 (45-45) and block3 (80-10). The probability of win-
1398 stay (A and B), latency of trial initiation (C and D), and action selection reaction time (E
1399 and F) are not significantly modulated by reward size. Dots represent the individual
1400 sessions.

1401

1402

1403

1404